Mineralogical analysis of the Oppia quadrangle of aAsteroid (4) Vesta: Evidence for occurrence of moderate-reflectance hydrated minerals

F. Tosi[a, *]

federico.tosi@iaps.inaf.it

A. Frigeri[a]

J.-Ph. Combe[b]

F. Zambon[a]

M.C. De Sanctis[a]

E. Ammannito[c, a]

A. Longobardo[a]

M. Hoffmann[d]

A. Nathues[d]

W.B. Garry[e]

D.T. Blewett[f]

C.M. Pieters[g]

E. Palomba[a]

K. Stephan[h]

L.A. McFadden[e]

H.Y. McSween[i]

C.T. Russell[c]

C.A. Raymond[j]

the *Dawn* Science Team

[a]INAF-IAPS Istituto di Astrofisica e Planetologia Spaziali, Via del Fosso del Cavaliere, 100, I-00133 Rome, Italy

[b]Bear Fight Institute, 22, Fiddler's Road, P.O. Box 667, Winthrop, WA 98862, USA

[c]Institute of Geophysics and Planetary Physics, University of California at Los Angeles, 3845 Slichter Hall, 603 Charles E. Young Drive, East, Los Angeles, CA 90095-1567, USA

[d]Max Planck Institute for Solar System Research, Justus-von-Liebig-Weg 3, D-37077 Göttingen, Germany

[e]NASA/Goddard Space Flight Center, Greenbelt, 8800 Greenbelt Road, MD 20771, USA

[f]The Johns Hopkins University Applied Physics Laboratory, 11100 Johns Hopkins Road, Laurel, MD 20723, USA

[g]Department of Earth, Environmental and Planetary Sciences, Brown University, 324 Brook Street, Providence, RI 02912, USA

elsevier_YICAR_11576

[h]Institute of Planetary Research, German Aerospace Center (DLR), Rutherfordstrasse 2, D-12489 Berlin, Germany

[i]Department of Earth and Planetary Sciences, The University of Tennesse, 1412 Circle Drive, Knoxville, TN 37996, USA

[j]NASA/Jet Propulsion Laboratory and California Institute of Technology, 4800 Oak Grove Drive, Pasadena, CA 91109, USA

*Corresponding author. Fax: +39 06 45488 702.

Abstract

Quadrangle Av-10 'Oppia' is one of five quadrangles that cover the equatorial region of aAsteroid (4) Vesta. This quadrangle is notable for the broad, spectrally distinct ejecta that extend south of the Oppia crater. These ejecta exhibit the steepest ('reddest') visible spectral slope observed across the asteroid and have distinct color properties as seen in multispectral composite images. Compared to previous works that focused on the composition and nature of unusual ('orange') ejecta found on Vesta, here we take into account a broader area that includes several features of interest, with an emphasis on mineralogy as inferred from data obtained by Dawn's Visible InfraRed mapping spectrometer (VIR). Our analysis shows that the older northern and northeastern part of Av-10 is dominated by howardite-like material, while the younger southwestern part, including Oppia and its ejecta blanket, has a markedly eucritic mineralogy. The association of the mineralogical information with the geologic and topographic contexts allows for the establishment of relationships between the age of the main formations observed in this quadrangle and their composition. A major point of interest in the Oppia quadrangle is the spectral signature of hydrous material seen at the local scale. This material can be mapped by using high-resolution VIR data, combined with multispectral image products from the Dawn Framing Camera (FC) so as to enable a clear correlation with specific geologic features. Hydrated mineral phases studied previously on Vesta generally correlate with low-albedo material delivered by carbonaceous asteroids. However, our analysis shows that the strongest OH signature in Av-10 is found in a unit west of Oppia, previously mapped as 'light mantle material' and showing moderate reflectance and a red visible slope. With the available data we cannot yet assess the presence of water in this material. However, we offer a possible explanation for its origin.

Keywords: Asteroids, surfaces; Asteroid Vesta; Spectrophotometry; Infrared observations

1 Introduction

At 525 km in mean diameter, Vesta is the second largest object in the main asteroid belt of our Solar System. Pyroxene absorptions are the most prominent visible-to-near infrared spectral features of Vesta (e.g., McCord et al., 1970; Gaffey, 1997; Binzel et al., 1997, and references therein), and the overall mineralogy is consistent with howardite–eucrite–diogenite (HED) meteorites (e.g., Consolmagno and Drake, 1977; Feierberg and Drake, 1980). In particular, spectra collected by the Dawn spacecraft's Visible InfraRed (VIR) mapping spectrometer (De Sanctis et al., 2011) at spatial scales ranging from tens of meters to tens of kilometers are consistent with a surface covered by a howardite-like regolith containing varying proportions of eucrite and diogenite at different locations (De Sanctis et al., 2012a, 2013).

The Oppia quadrangle (Av-10) is one of five quadrangles on Vesta that cover the equatorial region (Lon 288°–360°E, 78°–150°E IAU, Lat ±22°, Roatsch et al., 2012). It is named after *Oppia* (Lon 309.1°E, 99.1°E IAU, Lat 7.9°S), the quadrangle's second largest crater (diameter of ~37 km). Other impact craters with diameters in the range of 20–40 km in this quadrangle are *Lepida* and *Paulina*.

A thorough geologic mapping of the Av-10 quadrangle (Garry et al., 2014) established that the heavily cratered highlands in the far northeast are the oldest unit. These highlands represent some of the original crustal material on Vesta; they were excavated by one or more impacts to form the east–west elongated basin *Feralia Planitia* in the middle and the cratered plains unit in the west and southwest, all of which are Pre-Veneneian in age (Williams et al., 2014b). Two terrains characterized by ridge and trough systems are the *Saturnalia Fossae Formation*, a depression that cuts diagonally across the quadrangle from the far northwest to the center of the quadrangle, and the *Divalia Fossae Formation*, the equatorial trough system located in the southeast corner (Garry et al., 2014). Saturnalia and Divalia are Veneneian and Rheasilvian in age, respectively (Williams et al., 2014b). The youngest geologic units/features in Av-10 are several impact craters that have formed in the aforementioned terrains and are either Late Rheasilvian or Marcian in age (e.g., Lepida, Oppia, Paulina). The main geologic features of Av-10 are summarized in the geologic map adapted from Garry et al. (2014), shown in Fig. 1b.

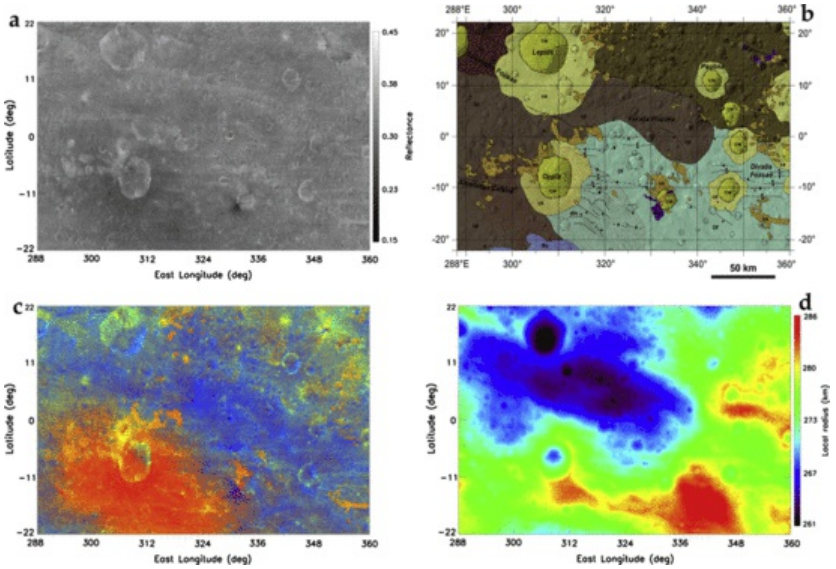

Fig. 1 Panel a: Reflectance map of quadrangle Av-10 Oppia, obtained through photometric correction of FC clear-filter data acquired in the HAMO and HAMO-2 mission phases. The map scale is 60 m/pixel. Panel b: Geologic map of Av-10 Oppia quad, adapted from Garry et al. (2014). The broad ejecta blanket extending south of Oppia is mapped as 'dark mantle material' (*dm*) because it appears dark orange to red in the 'Clementine' color composite. Patches of 'light mantle material' (*lm*) are found locally in the vicinity of Oppia and elsewhere in the quad. Panel c: RGB composite of the Av-10 Oppia quadrangle made from FC color ratios: $R = 438$ nm/749 nm, $G = 749$ nm/917 nm, $B = 749$ nm/438 nm ('Clementine' color composite). Color ratios may enhance differences in ~~material and~~ composition. Combined with the reflectance map of Vesta's surface, this color-ratio composite shows: (1) bright material in yellow/green, (2) dark material in bluish/violet, and (3) spectrally distinct ejecta in red/orange. Panel d: Portion of the digital terrain model (DTM produced by DLR, 2013-05-24) derived from FC images acquired in HAMO and HAMO-2, at a scale of 64 pixels/deg. The rainbow color palette follows topography (local radius), with the highest elevations in red and the lowest terrains in dark blue/violet. (For interpretation of the references to color in this figure legend, the reader is referred to the web version of this article.)

Oppia crater is associated with broad, spectrally distinct ejecta that stand out even in low-resolution maps. The ejecta blanket of Oppia is mapped as 'dark mantle material' because it has relatively low reflectance and appears dark orange to red in Dawn Framing Camera (FC) 'Clementine' color-ratio composite images, with a diffuse, gradational contact distributed to the south across the rim of the Rheasilvia giant impact basin (Garry et al., 2014). Another remarkable multispectral unit in Av-10 is 'light mantle material', which appears as light orange in the FC color-ratio image. Light mantle material occurs in small, individual patches showing irregular shapes, typically associated with the rims of both fresh and degraded impact craters (Garry et al., 2014). Unlike what is typically observed for the light mantle unit, dark mantle material is not found in smaller patches.

Oppia shares several similarities with the crater Octavia, located at roughly the same latitude, but almost directly on the opposite side of Vesta in the Av-8 Marcia quadrangle (De Sanctis et al., this issue). Octavia also shows distinctive diffuse dark orange ejecta, similar to the dark mantle material found in Oppia. Furthermore, Oppia and Octavia both overlap the equatorial troughs and are mapped within the Divalia Fossae Formation on opposite sides of Vestalia Terra. Octavia has a similar crater diameter (~35 km) and has an ejecta blanket that is relatively evenly distributed with a diffuse, gradational boundary as observed at Oppia (Le Corre et al., 2013; Williams et al., 2014a; Schäfer et al., 2014).

Prior to Dawn, rotationally resolved ground-based near-IR spectra of Vesta suggested that albedo variations might be linked to surface compositional heterogeneity. In particular, Gaffey (1997) first noticed a decrease in ratio of 2-μm/1-μm pyroxene band area as Vesta rotated, and suggested the presence of a large olivine-rich unit on the surface. This unit has the reddest spectral color over the entire surface of Vesta observed by the Hubble Space Telescope (Li et al., 2010), with a shallower band depth than the background surface. In Dawn Framing Camera color maps, this feature corresponds to the Oppia crater and its diffuse ejecta blanket (Reddy et al., 2013). The band depth as measured by the FC 0.75-μm/0.92-μm reflectance ratio for the Oppia region is also shallower than the average surface of Vesta (Reddy et al., 2012). Due to low albedo, red slope and weaker pyroxene bands, Li et al. (2010) interpreted this region to be space weathered.

Mineralogical studies based on Dawn/VIR data shed light on the presence of diffuse areas of hydrous material (De Sanctis et al., 2012b) and specific classes of terrains such as bright- and dark-material units seen at the local scale (Jaumann et al., 2012; Palomba et al., 2014; Zambon et al., 2014; Longobardo et al., 2014; Tosi et al., 2014). VIR data collected at a high spatial resolution were also used to provide definitive evidence of local concentrations of olivine (Ammannito et al., 2013; Ruesch et al., 2014) and orthopyroxene on a topographic high (Buczkowski et al., 2014; De Sanctis et al., 2014), supporting the hypothesis of localized magmatic intrusions on Vesta. However, unlike what was initially suggested from Earth-based observations, no olivine has yet been detected in the Oppia region.

Here we present a detailed mineralogic study of the Av-10 Oppia quadrangle both as a whole and with an emphasis on selected surface units. Most of our mineralogical analysis is carried out on the basis of the latest calibrated VIR near-IR spectra. The combination of VIR data with FC imagery showing a higher spatial resolution enables accurate correlation of spectral units with geologic units and topography. In addition, we also take advantage of the thermal infrared range measured by VIR to derive a spatially-resolved temperature map of Av-10. These are clear advances compared to previous works, which together allow for both a broader understanding of the processes that gave rise to the currently observed composition, and a better correlation with processes that are found in other quadrangles on Vesta.

2 Data

Launched on 27 September 2007, the Dawn spacecraft entered orbit around Vesta on 16 July 2011, following a polar trajectory (Russell et al., 2012). The orbital mission of Dawn at Vesta was divided into four main phases: Survey, High-Altitude Mapping Orbit (HAMO), Low-Altitude Mapping Orbit (LAMO), and High-Altitude Mapping Orbit 2 (HAMO-2), prior to departure on 5 September 2012. Each phase had a different length and was carried out in a different altitude range, with spatial resolution depending on the altitude over the mean surface: from the Survey orbit, the average pixel resolution was 0.676–0.719 km for VIR and 0.252–0.268 km for FC; from the HAMO orbit it was 0.165–0.205 km for VIR and 0.062–0.076 km for FC; in the LAMO phase it was 0.043–0.075 km for VIR and 0.016–0.028 km for FC; and finally in the HAMO-2 period it was 0.161–0.206 km for VIR and 0.060–0.077 km for FC (very similar to the resolution achieved in the previous HAMO phase). However, it should be noted that the different stages of the Dawn mission at Vesta occurred under changing illumination conditions, with the phase angle increasing from Survey to LAMO, along with a variable coverage of the surface. Largest coverage and most favorable illumination conditions for spectroscopy were achieved in the Survey phase, even though the spatial resolution was relatively low when compared to the subsequent stages. The most limited spatial coverage and lowest signal-to-noise ratio (SNR) were obtained in LAMO, which in the case of VIR make these data less optimal for use and interpretation, compared to those obtained in the other phases.

The data used in this paper have been obtained by the two imaging systems onboard Dawn: VIR and FC. The VIR instrument (De Sanctis et al., 2011) is an imaging spectrometer with an overall spectral range from 0.25 to 5.1 μm, designed to determine the mineral composition of surface materials in their geologic context, and to derive spatially-resolved thermal maps of the asteroid on its dayside in locations with temperatures above ~180 K (Tosi et al., 2014). The FC (Sierks et al., 2011) has a broad-band clear filter and 7 narrow-band filters (0.4 to 1.0 μm) that obtained near-global coverage of the surface revealing detailed albedo and color variations. FC images have also been used to derive an accurate shape model of the asteroid (Jaumann et al., 2012).

3 Tools and techniques

3.1 Spectral parameters

In the near-IR domain, Vesta's spectral reflectance is dominated by two pyroxene absorption bands, respectively centered near wavelengths of ~1 μm and ~2 μm, and commonly referred to as Band I and Band II (hereafter BI and BII). VIR spectra at spatial scales ranging from tens of meters to tens of kilometers are consistent with a surface covered by a howardite-like regolith containing varying proportions of eucrite and diogenite at different locations (De Sanctis et al., 2012a, 2013). Mineralogically, eucrites contain primarily anorthitic plagioclase and low-Ca pyroxene with augite exsolution lamellae, while diogenites are predominately magnesian orthopyroxene (Burbine et al., 2001).

To study the spectral properties of the Oppia quadrangle and to understand the mineralogical composition and the physical characteristics of the regolith effective grain size, we introduce in our analyses spectral parameters such as the band center (BC) and the band depth (BD). The band center is the location of the reflectance minimum inside the band after the spectral continuum removal, while the band depth is defined in the manner of Clark and Roush (1984): $1 - R_b/R_c$, where R_b and R_c are the reflectance of the band and the spectral continuum at the BC.

The spectral positions of the Band I and Band II centers (hereafter BCI and BCII) determine the degree of diogenitic, howarditic or eucritic composition, with shorter and longer wavelengths associated with diogenite-rich and eucrite-rich minerals, respectively, due to the more Ca- and Fe-rich nature of eucrite pyroxenes compared to diogenite pyroxenes (Gaffey, 1976). Band centers are also used to characterize material as having howardite, eucrite or diogenite (HED) affinities (e.g., Cloutis and Gaffey, 1991; Burbine et al., 2001). Therefore, plotting BCII values versus BCI values is a powerful way to identify and separate different lithologies on Vesta. Indeed, the displacement of the pyroxene band centers is sensitive to temperature variations (e.g., Burbine et al., 2009), even though, given the usual range of daytime temperatures recorded on Vesta, this effect is essentially negligible in VIR data (Longobardo et al., 2014).

Band depths are indicative of pyroxene composition and abundance, the presence of opaque minerals or other phases, and in principle also depend on the grain size distribution (e.g., Adams, 1974; Clark, 1999; Cloutis et al., 2013). The analysis carried out by Zambon et al. (2014) and (The word "and" should not be colored in blue, as it is not a link to a bibliographic reference.) Palomba et al. (2014) on the bright- and dark material units, respectively, found that on Vesta, band depths generally increase in bright materials with respect to the surrounding terrains, and decrease in dark materials. In particular, Palomba et al. (2014) reported that BII that can be also largely reduced in very dark materials, but never completely suppressed. From these works based on VIR spectroscopic data, it was established that the grain size of Vesta's regolith has an average value of 25 μm, with an upper limit of 45 μm. Therefore it is unlikely that the variations in band depths that we observe can be attributed to substantial variations in the grain size.

Unlike band centers, band depth values are affected by the illumination and observation geometry, hence a photometric correction is required to allow a proper interpretation. In VIR data discussed here, this correction has been applied according to the procedure described in Longobardo et al. (2014), which first removes the local topography effects by means of the Akimov disk function (Akimov, 1975; Shkuratov et al., 1999) and then removes the reflectance variations due to the different observation geometry

by means of the phase function retrieved by Longobardo et al. (2014). In particular, in this work we consider BD values corrected at 0° phase angle.

The weak 2.8-μm feature is diagnostic of OH-bearing material. Mapping of the absorption band depth of hydroxyl relies on the calculation of a difference between a linear continuum anchored at the two shoulders of the band and the reflectance at the center (Combe et al., this issue-a). In principle, the presence of H_2O could be investigated by examining absorption in the 3.0–3.1 μm range. Unfortunately, even when using the VIR data calibrated with the latest sensitivity function, this part of the spectrum is affected by substantial calibration residuals especially in the HAMO and HAMO-2 phases, which together provided the majority of the VIR data discussed here. Thus, data acquired in the Survey phase at lower spatial resolution are more suitable to undertake this analysis.

3.2 Spectral maps

Frigeri et al. (this issue-a) provides details about how VIR spectral parameters were derived, filtered and mapped. In particular, VIR spectral indices cover the Survey, HAMO, LAMO, and HAMO-2 mission phases, and were produced from single hyperspectral images and interpolated on a grid with a fixed resolution of 100 m/pixel (Frigeri et al., this issue-a). The mineralogical maps of the entire quadrangle, on which our analysis dwells, are based on the position of the center of the pyroxene bands BI and BII, and on their associated band depths. Stripes and spurious values, disconnected from the geologic context, may occur in these maps, as a consequence of the fact that BC and BD values were not optimized for specific quadrangles but rather were filtered for the entire surface of Vesta (Frigeri et al., this issue-a), which may result in residual artifacts. However, our analysis has further refined these maps, excluding values that are not spatially coherent or are clearly the counterpart of instrumental artifacts.

FC color filter data were used to create an enhanced color mosaic using ratios comparable to the ones used in analysis of Clementine images of the Moon (red: 750/430 nm, green: 750/920 nm, blue: 430/750 nm) (Pieters et al., 1994). The 'Clementine' color composite map is of interest to evaluate local spectral variations at high spatial resolution, which may trace variations in composition. In this presentation, dark materials appear dark bluish/violet and bright materials are yellow–green, with intermediate albedo surfaces appearing as cyan. Comparing Clementine color data and VIR spectral maps is indeed a powerful way to highlight possible correlations between mineralogy and spectrally distinct structures seen in color imagery with higher spatial resolution. On the other hand, while the Clementine color code proved to be optimal for Moon data, it may not necessarily be the best presentation to trace compositional differences in other rocky bodies of the Solar System. For this reason, in this work we explored the Oppia region using also one alternative FC color scheme, to investigate the existence of spectral textures that would otherwise remain elusive or hidden.

The presence of intrinsically dark and bright material units can be evaluated by means of albedo or reflectance maps. In our case, we considered two reflectance indicators: (1) a reflectance map obtained in the FC clear filter during the HAMO and HAMO-2 mission phases, at a scale of 60 m/pixel (Roatsch et al., 2012; Schröder et al., 2013), and photometrically corrected by means of the Akimov function (Akimov, 1975),[1] and (2) a reflectance map derived from VIR data at 1.4 μm with a resolution of 200 m/pixel, photometrically corrected by means of the Akimov disk function (Akimov, 1975; Shkuratov et al., 1999) (Combe et al., this issue-a). To increase the SNR, the latter map relies on VIR data acquired in the Approach, Survey, HAMO and HAMO-2 mission phases. Overall, these maps allow comparison of surfaces on the basis of their inherent reflectance (i.e., bright vs. dark material).

Because the 1.4-μm wavelength in VIR data is not affected neither by spectral signatures known or expected on the surface of Vesta, nor by VIR instrumental artifacts, it turns out to be optimal to sample the continuum in a spectral region dominated by solar reflection. Its use in conjunction with the map of the weak 2.8-μm band depth obtained at the same spatial scale (Combe et al., this issue-a) is key to highlight correlations between reflectance and abundance of OH-bearing phases. In general, Vesta shows a linear and diffuse anti-correlation between surface reflectance and the 2.8-μm band depth (McCord et al., 2012). However, some variability is found within this trend. Our analysis uses tools such as the relationship between the measured reflectance and the measured/modeled reflectance ratio, to highlight the occurrence of local regions that substantially deviate from the ideally linear trend. Furthermore, we use a four-color map to merge the 1.4-μm reflectance map and the 2.8-μm BD map into a single composite map, where colors are indicative of both reflectance and abundance of hydrous species at the same time.

3.3 Other maps: geologic map, topographic map, temperature map

The availability of the geologic map of Garry et al. (2014) allows us to associate the composition of the main surface units of the Oppia quadrangle to their relative geologic timescale and therefore achieve a clear picture about the sequence of events that led to the mineralogy that is observed on Vesta today. A digital terrain model (DTM) of the Oppia quadrangle derived from FC clear-filter data, with a resolution of 48 pixels/deg or ~92 m/pixel (Jaumann et al., 2012) is also used to cross-check correlations between composition and topography, and to draw vertical profiles of composition as a function of the local elevation, which aid in the interpretation.

The long-wavelength range of VIR sensitivity, 4.5–5.1 μm, is used to systematically retrieve surface temperatures. These data were used both to produce global maps and to investigate in detail the behavior of local-scale features (Tosi et al., 2014). The motivation for such an investigation lies in a search for thermal anomalies, that is, regions whose response to insolation differs from the average behavior of the quadrangle and of the asteroid as a whole. In general, the surface of Vesta has a very low thermal inertia (Capria et al., 2014), but deviations from this rule are found at the local scale, e.g., due to variations in regolith thickness, density, or thermal conductivity. For this reason, we also included a map of surface temperature of the Av-10 quadrangle derived from VIR infrared data.

In all maps, including the spectral maps described in the previous sub-section, longitudes are given in the Dawn Claudia coordinate system (Russell et al., 2012; Roatsch et al., 2012; Li, 2013), rather than in the International Astronomical Union (IAU) coordinate system (Claudia coordinate system = [IAU longitude] – 150°).

3.4 Spectral unmixing

To further investigate the composition of the Oppia crater region, we applied spectral unmixing to VIR HAMO and HAMO-2 data. Based on the spatial scale of these observations (~0.18 km/px), we chose to employ a linear spectral unmixing model. The approach is described in the work by Zambon et al. (submitted~~in preparation~~),(In the references list, please add the following reference:

Zambon, F., Tosi, F., Carli, C., De Sanctis, M.C., Blewett, D.T., Palomba, E., Longobardo, A., Frigeri, A., Ammannito, E., Russell, C.T., Raymond, C.A., 2015b. Lithologic variation within bright material units on Vesta revealed by linear spectral unmixing. Icarus, submitted.) to which the reader is referred for more details. Briefly, it is assumed that each measured spectrum is the result of a linear combination of three spectral endmembers. These are automatically selected among 11 laboratory samples representative of the overall surface mineralogy: 6 eucrites, 3 diogenites and 2 olivines, plus a featureless component (straight horizontal line) that accounts for the reduction of band depth caused by a neutral dark material. Since howardite meteorites are a mixture of eucrite and diogenite in varying proportions, we do not consider howardite among the endmembers. The spectra are cut out in the region between 0.6 and 2.5 μm, which is diagnostic for the main lithologies found on Vesta and offers at the same time a reliable responsivity and a high SNR in VIR data. The algorithm is not bound to select different lithologies at one time: the linear combination providing a best fit (i.e., the one that minimizes the chi-square value) may be made up of two eucrites and one diogenite, two eucrites and the featureless component, three eucrites, etc. The combination is constrained such that the sum of the relative abundances of the three endmembers must be equal to 1.

The accuracy of this technique has been tested on laboratory samples of HED meteorites and olivine, whose relative abundance was known a priori (Zambon et al., submitted~~in preparation~~). Neither albedo nor the slope of the spectral continuum are taken into account in the search for a best fit, because the slope is first removed from all spectra. Therefore, the analysis is carried out mainly on the basis of the position, shape and depth of the pyroxene absorption bands, which discriminate between the possible lithologies.

4 General mineralogy of Av-10

4.1 Reflectance, colors and topography

First, we summarize the main features that have been described in the Oppia quadrangle based on FC data, providing a high-resolution context for subsequent analysis and interpretation of mineralogy data. To do so, we rely on a comparison between four maps, shown in Fig. 1: a reflectance map; a Clementine color composite map; the geologic map produced by Garry et al. (2014); and a DTM.

From the reflectance map (Fig. 1a), whose values range from 0.15 to 0.45, one can easily infer the existence of bright and dark materials, which stand out as having substantially higher or lower reflectance than the quadrangle's average value of 0.30. The highest reflectance materials are generally associated with impact craters, including both prominent examples (e.g., Lepida, Oppia) and smaller craters. Sometimes bright units appear in the form of crater wall material and slope material, i.e. outcrops sliding inward from the rim of the crater, and sometimes in the form of radial material (ejecta) (for a classification of bright materials on Vesta, see Mittlefehldt et al., 2012). In Av-10, the presence of dark material units is less frequent: the most notable example is provided by the southwestern rim of an unnamed crater, which is medium in size (when compared to the largest craters in the quadrangle) and located at 12.5°S, 333.7°E. Other moderate reflectance materials can be observed at various locations. In particular, a series of moderately reflective patches are found outside of the western and northwestern edge of Oppia, and have the appearance of material generated following the impact. Similar diffuse patches are also found elsewhere in the quadrangle, e.g., in the aforementioned unnamed crater showing a dark material deposit, and in the southeastern corner of the quadrangle.

Geologic mapping of Oppia Quadrangle Av-10 (Fig. 1b, adapted from Garry et al., 2014) shows that this area is a junction of key geologic features that preserve a rough geologic history of asteroid Vesta and is a contained case study to define a relative geologic timescale for Vesta. Quadrangle Av-10 contains geologic map units that are representative of each of the vestan time-stratigraphic systems and time periods: cratered highlands terrain (*ch*), cratered plains material (*cp*), Saturnalia Fossae Formation trough terrain (*Sf*), Divalia Fossae Formation trough terrain (*Df*), Rheasilvia Formation – smooth terrain (*Rs*), crater wall and ejecta (*cw*, *ce*), dark crater rays (*dcr*), and light and dark mantle (*lm*, *dm*).

The Clementine color composite map (Fig. 1c) shows the usual bluish/violet, yellow–green and cyan shades found in most of the vestan surface. Notable examples are the northern wall of the craters Lepida and Oppia, the ejecta of a 5-km unnamed crater located just outside the northern rim of Oppia (which we will name 'Oppia B' hereafter), and the ejecta of some small unnamed craters in the northeastern corner of the quadrangle. However, the Av-10 quadrangle also offers important exceptions, because the Oppia ejecta to the south show colors in the composite image ranging from dark orange to red. This dark orange and red material correlates with diffuse areas with lower reflectance than the average reflectance of the quadrangle and thus classified as 'dark mantle material' (Garry et al., 2014). This prominent multispectral unit has the reddest visible continuum slope across the entire asteroid (Li et al., 2010). Moreover, there are other patches of light orange material, with well-defined edges. The latter type of material, mapped as 'light mantle material', has been interpreted as impact ejecta, possibly glassy impact melt (Le Corre et al., 2013; Garry et al., 2014). Its presence near Oppia, and in particular the morphology observed in the area west of the crater, suggests that this material was emplaced as a result of the event that formed Oppia itself. Other patches of light mantle material are found in Av-10 at greater distances from Oppia: for example, in a terrain located northwest of the unnamed crater hosting a local concentration of dark material, whose shape reveals an origin disconnected from the Oppia event.

One intriguing finding that emerges from the comparison between the Clementine color composite image (Fig. 1c) and the reflectance map (Fig. 1a) is that the light mantle material may be associated with local concentrations of moderate reflectance material. This is especially the case for light mantle material found near Oppia, while it is less obvious for light mantle material located at a greater distance, especially where it stretches out in the far north, grouped in patches of relatively small size. These

northern small spots do not have a~~n appreciable~~considerable contrast in reflectance with respect to surrounding terrains.

Fig. 1d is a portion of the DTM of Vesta for the Av-10 quadrangle, where the rainbow palette reflects the local topography. The maximum topographic relief that occurs in this quadrangle is 24 km, with the deepest part corresponding to Lepida crater's floor (~262 km in local radius) and the highest elevations (up to 286 km in local radius) concentrated in the southeast. Feralia Planitia is surrounded by topographically higher cratered terrain in the far northeast and a relatively smoother, faulted terrain along the southern border. Feralia Planitia has been altered by structural troughs as well as two impact events, Lepida and Oppia (Garry et al., 2014). The available datasets permit investigation of possible correlations between variations in reflectance and/or color, and the presence of hills and depressions. The topographic map also serves as a monitoring tool, allowing one to determine whether an observed variation in spectral indicators is reliable and not simply due to the combination of local topography and instantaneous solar illumination (see Section 3.1).

4.2 Pyroxene band centers

As discussed in Section 3.1, a plot of BI center ~~versus~~, BII center as measured by VIR is a powerful way to identify and separate the main lithologies on Vesta. Such a plot for the Av-10 Oppia quadrangle is shown in Fig. 2.

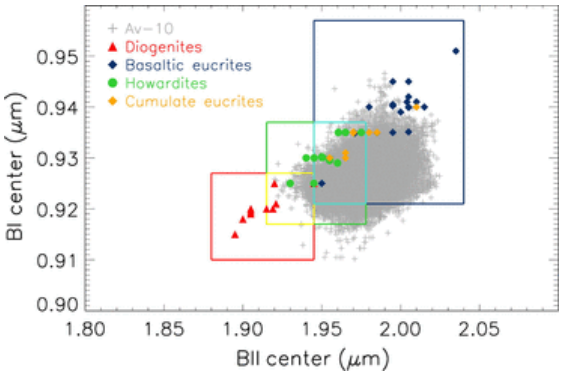

Fig. 2 Scatterplot of pyroxene BI and BII centers for Av-10. The gray points represent the distribution of the band centers as measured by VIR throughout the Vesta orbital mission. Colored points are the band center values measured in lab for several HED meteorites covering different lithologies (from De Sanctis et al., 2013). The blue and red boxes, respectively, delimit the regions of the two categories of eucrites and diogenites, determined on the basis of laboratory measurements performed on a large number of HED meteorite samples. The green square in the center identifies the intermediate category of howardites, with cyan and yellow rectangles that mark the area of eucrite-rich howardites and diogenite-rich howardites, respectively. (For interpretation of the references to color in this figure legend, the reader is referred to the web version of this article.)

BC values in Av-10 span the overall range 0.91–0.95 μm for BI and 1.92–2.03 μm for BII. The distribution clearly demonstrates that most of the Av-10 quadrangle is dominated by a eucritic and howarditic mineralogy, with a minority of the surface belonging to the diogenite-rich howardites region, and no pixels falling into the category of pure diogenites. We next assess the spatial context of the mineralogical variations within the quadrangle.

In Fig. 3 we show a map of BCI and BCII, with pseudo-colors related to the band center value. The red color corresponds to values compatible with a howarditic lithology, while the blue color corresponds to band center values shifted toward~~s~~ longer wavelengths and therefore consistent with a eucritic lithology. The BCII map displays better spatial coherence than the BCI map, due to lower instrumental noise in the 2.0-μm portion of the VIR data in comparison to the 0.9-μm region. From the BCII map we can perceive clear trends in the mineralogy. The older northeastern cratered highlands, including Paulina crater and the northern half of Lepida to the west, have a howarditic mineralogy. The younger southwestern cratered plains, including Oppia, Albalonga Catena and material related to the Divalia Fossae formation, exhibit an eucritic lithology. Feralia Planitia, which is located roughly in the middle of the quadrangle at the boundary between these opposing geologic units, also has a eucritic affinity, similar to the area around Oppia. Diogenite-rich howardite, with BCI values ranging between 0.91 and 0.92 μm and BCII values ranging between 1.92 μm and 1.94 μm, is only found in a few sites, all located in the northeast corner of the quadrangle, corresponding to the heavily cratered highlands. The geographical distribution of the band centers fits into a broader context, with howarditic material that connects to adjacent quadrangles to the north and east: Av-5 Floronia, Av-2 Bellicia, and Av-6 Gegania (Combe et al., this issue-b; Longobardo et al., this issue); and the eucritic material associated with Oppia ejecta that continues toward~~s~~ the neighboring southern quadrangles Av-13 Tuccia and Av-14 Urbinia (Zambon et al., this issue).

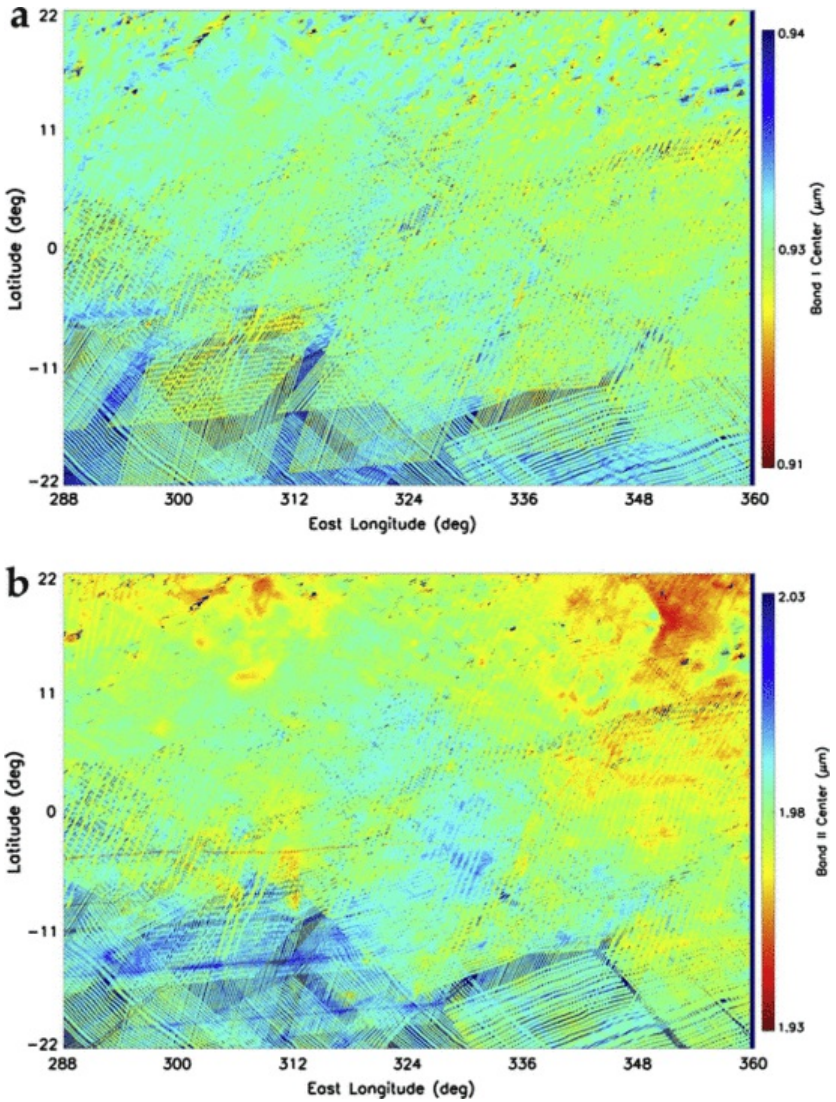

Fig. 3 Distribution of the pyroxene Band I center (panel a) and Band II center (panel b) values across the Oppia quad, derived from VIR data. The relative spectral position of BCI and BCII expresses the degree of diogenitic, howarditic or eucritic composition, with shorter and longer wavelengths associated with diogenite-rich and eucrite-rich units, respectively. The overall mineralogy of Oppia spans from howarditic (red) to eucritic (blue), with yellow, green and cyan colors corresponding to transition areas between these two main lithologies. In both distributions, but more distinctly in the BCII distribution, latitudinal gradients are found: the northeastern part of Av-10 (older) is dominated by howardite, whereas the southwestern part (younger), including Oppia and its ejecta blanket, has a eucritic mineralogy. (For interpretation of the references to color in this figure legend, the reader is referred to the web version of this article.)

We next investigate correlations between the band centers and the reflectance. Fig. 4 shows scatterplots of the VIR 1.4-μm reflectance versus BCI and BCII values. In general, the distribution of BCI points has a very large spread and there is no correlation with reflectance. However, the distribution of BCII shows a weak anticorrelation between the value of the reflectance and the value of the band center, although there is a large dispersion. This means that higher values of BC (eucritic) are associated with lower values of reflectance. BC values do not depend on the illumination/observation geometry, and we can also rule out a strong dependence on surface temperature (Longobardo et al., 2014). The tendency for lower reflectance areas to correlate with eucritic mineralogy fits with what is known from meteorite studies: eucrite-rich assemblages are on average darker than diogenite-rich materials, with howardites showing intermediate reflectance values. This correlation with reflectance is not observed in our BCI

map likely due to the greater instrumental noise that affects the 0.9-μm region in VIR data. Moreover, in the BCII image, we can identify at least one lobe of points characterized by a significantly lower reflectance than the average, showing band center values comprised between 1.97 μm and 1.99 μm and hence a eucritic composition.

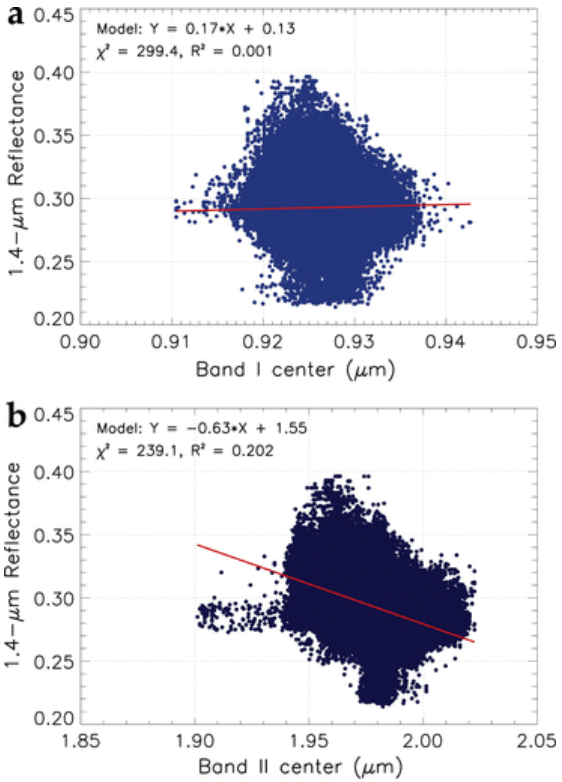

Fig. 4 Scatterplot of 1.4-μm reflectance as a function of the wavelength position of the BI center (panel a) and BII center (panel b). In both distributions, a linear fit model is superimposed on the distribution (red line). In the case of BCI, no correlation exists between the two variables, whereas the BCII distribution shows a weak anti-correlation with reflectance, with the wavelength position of darker materials shifting toward longer wavelengths. (For interpretation of the references to color in this figure legend, the reader is referred to the web version of this article.)

As a further means of investigation, in Fig. 5 we considered three profiles drawn from the same point in the floor of crater Oppia and extending to the northwest (NW), west–northwest (WNW), and west (W). These traverses were selected to sample Oppia ejecta that are associated with the light mantle map unit, which appears light orange in the Clementine color composite image. Using the DTM allows one to extract a vertical cross-section, highlighting differences in composition as a function of elevation and distance along the traverse.

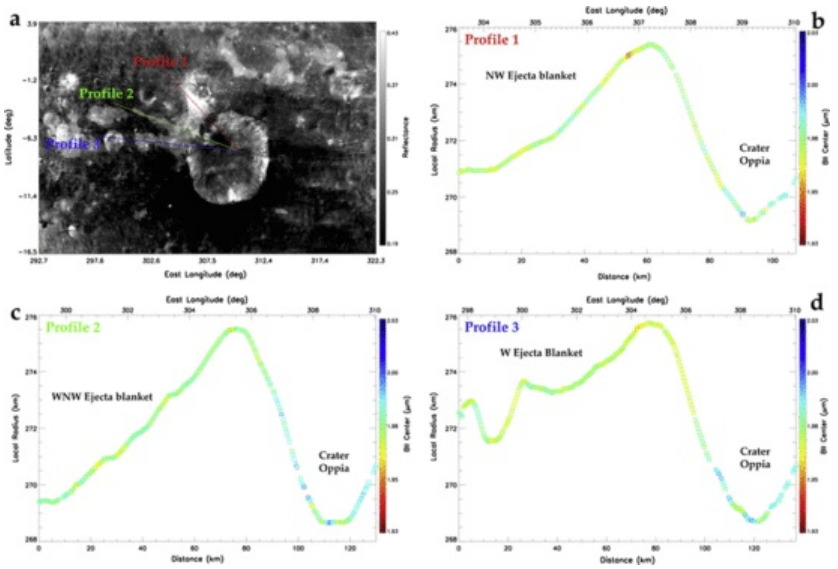

Fig. **(If needed, I have the high-resolution (1200 dpi) version of this figure. Please contact me to let me have instructions to upload the high-res file.)** **5** Panel a: Topographic profiles plotted as lines extending from Oppia towards the NW (red line), WNW (green line) and W (blue line), respectively. Panels b–d: For each of the three cross-sections the vertical profile (local radius in km) is shown as a function of both longitude and distance from the westernmost point of the traverse. The color scale is calibrated according to the BCII map shown in Fig. 3b: shades from green to blue highlight a eucritic mineralogy, while shades from green to red mark a howarditic composition. The floor of crater Oppia is consistent with a eucritic mineralogy, which is also found outside, in NW ejecta that overlap the region of the 5-km Oppia B crater. By contrast, the mineralogy of the W ejecta, as well as of the western rim and western inner wall of the crater, is shifted towards howardite, with WNW ejecta representing an intermediate composition. (For interpretation of the references to color in this figure legend, the reader is referred to the web version of this article.)

The result is shown in Fig. 5b–d, where profiles are colored according to the BCII value, in turn related to mineralogy. Referring to the same color scheme of Fig. 3b, the range of band center values found in the profiles is between 1.95 μm and 2.00 μm, corresponding to eucrite and eucrite-rich howardite compositions. While the floor of the crater Oppia has a eucritic composition, the composition may change with distance away from the crater's center. In the NW direction (Fig. 5b) the composition remains eucritic outside the crater. To the west (Fig. 5d), compositions consistent with eucrite-rich howardites are found (including the rim of the crater and the inner wall). The WNW profile (Fig. 5c) shows compositions intermediate between the other two.

4.3 Pyroxene band depths

Fig. 6 shows histograms related to the frequency of the band depth I and band depth II (hereafter BDI and BDII) values measured across the Oppia quadrangle, sampled with a 0.01 bin width.

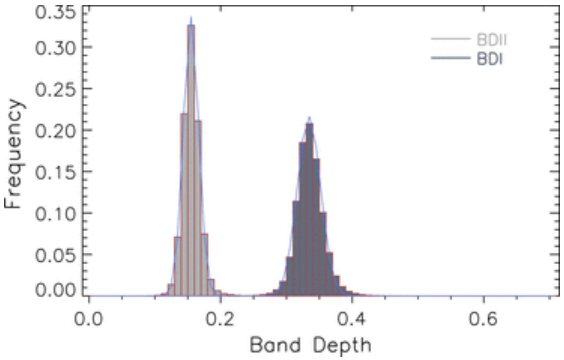

Fig. 6 Histograms of the Band I depth and Band II depth values measured across Av-10 quad (after photometric correction). A Gaussian fit is superimposed in the light blue color. Most frequent values are in the range 0.27–0.40 (average value 0.34) for BDI and 0.12–0.19 (average value 0.16) for BDII. (For interpretation of the references to color in this figure legend, the reader is referred to the web version of this article.)

As expected from the typical spectral profile of pyroxenes, BDI is greater than BDII, with most common values in the range 0.27–0.40 (average value 0.34) for BDI and 0.12–0.19 (average value 0.16) for BDII. Furthermore, the BD histograms have a

Gaussian shape. Because the band depth values are a function of the reflectance, with bright materials displaying deeper pyroxene bands than dark materials, a Gaussian or quasi-Gaussian distribution in the band depths reveals that the Oppia quadrangle presents a balanced budget between bright and dark material. For comparison, in other quadrangles of Vesta (also adjacent to Av-10), the observed statistics show a different distribution (e.g., Zambon et al., this issue; De Sanctis et al., this issue).

Fig. 7 reveals a map of the BDI and BDII values across the Oppia quadrangle. First, a comparison with the topographic map ~~shown in~~ of Fig. 1d shows that the band depth in most cases does not follow the trend of the topography, suggesting that the photometric correction has been successful in removing the effects of topographic slope (see Section 3.1). In general, it is observed that low BD values are associated with low-reflectance material, which appears bluish-violet in the Clementine presentation, such as the dark crater-ray material in the center of the southern half of the quadrangle and in much broader terrains as Feralia Planitia in the northern half of the quadrangle. A large area of low BD values (on average, BDI = 0.323 and BDII = 0.158) is associated with the dark mantle material, i.e., the prominent spectrally distinct unit that stretches south of Oppia. On the other hand, high BD values generally match with bright material, yellow–green in the Clementine color composite image. In particular, the maximum values in the Av-10 quadrangle are found in the borderland between the craters Oppia and Oppia B. Oppia itself has large spectral variations within its walls and floor. The rim and part of the wall close to the rim show high BD values (on average, BDI = 0.364 and BDII = 0.195) not always associated with outcrops of bright material, whereas the floor exhibits significantly smaller values. Other areas with a high BD value are scattered throughout the quadrangle, and are found particularly in the northeastern part that is characterized by cratered, howarditic highlands.

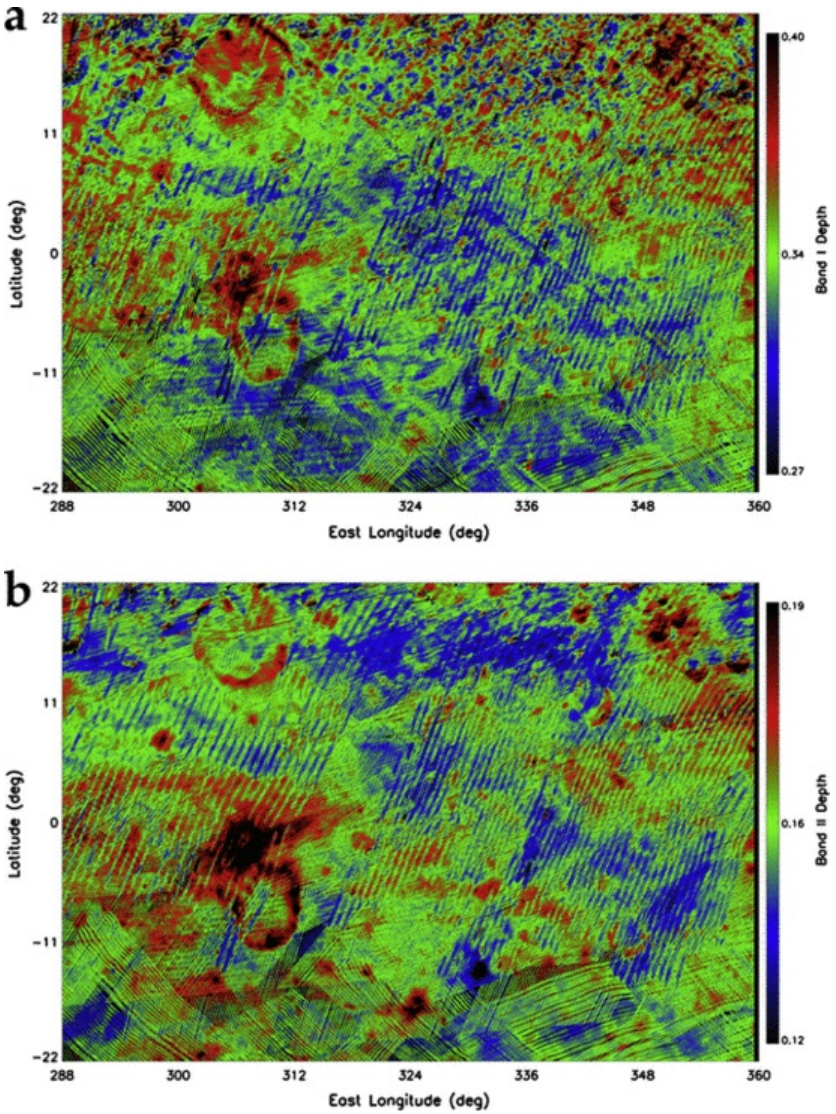

Fig. (If needed, I have the high-resolution (1200 dpi) version of this figure. Please contact me to let me have instructions to upload the high-res file.) 7 Distribution of the pyroxene Band I depth (panel a) and Band II depth (panel b) values across the Oppia quadrangle, derived from VIR data. Pyroxene BD are sensitive to the regolith grain size and to the presence of opaque contaminants. The overall distribution spans from lower depth (dark blue to blue) to greater depth (red to dark red). The dark mantle material associated with the prominent, spectrally distinct ejecta south of Oppia crater, has shallower pyroxene BD. Small values are also correlated with low reflectance material throughout the quadrangle. The Oppia crater has large spectral variations within its walls and floor: BD are shallower on the floor and stronger in the rim and walls. The largest BD values match the ejecta of the Oppia B crater, and in other scattered locations. (For interpretation of the references to color in this figure legend, the reader is referred to the web version of this article.)

We next evaluate the possible correlation between the 1.4-μm reflectance and pyroxene BD values. Fig. 8a is a scatterplot of 1.4-μm reflectance measured by VIR as a function of BDI and BDII values. As revealed by the chi-square, the distribution is highly non-linear, and the correlation between reflectance and BD is weak or absent. However, one can recognize the existence of trends. A lobe of points has low reflectance and low BD values, a typical characteristic of dark material units (having first excluded shadowed areas); a minority portion of moderate reflectance material shows the maximum BD values; and finally another minor set of points has high reflectance values and intermediate BD values. By mapping the ratio between the measured 1.4-μm reflectance and the BDII/1.4-μm linear approximation (Fig. 8b), one can see that points with BDII values significantly lower than the linear fit in general correspond to the area of the Oppia's eucritic ejecta and extend to the dark crater ray material, but also affect more distant

terrains as Feralia Planitia, Divalia Fossae and the crater Aconia. On the other hand, the 1.4-μm values well above the linear fit are generally found in the northern area of Av-10, including craters Lepida and Paulina. However, a detailed analysis of the Oppia crater area shows that this behavior also includes the 5-km Oppia B crater with bright material, and the bright slope material that is seen slipping down the southern rim of Oppia. Other examples include patches west of the crater that correspond to local concentrations of moderate reflectance material. In summary, despite the large spread, the distribution of reflectance vs. BD values confirms that high- and moderate-reflectance materials are associated with enhanced pyroxene BD compared to low-reflectance material.

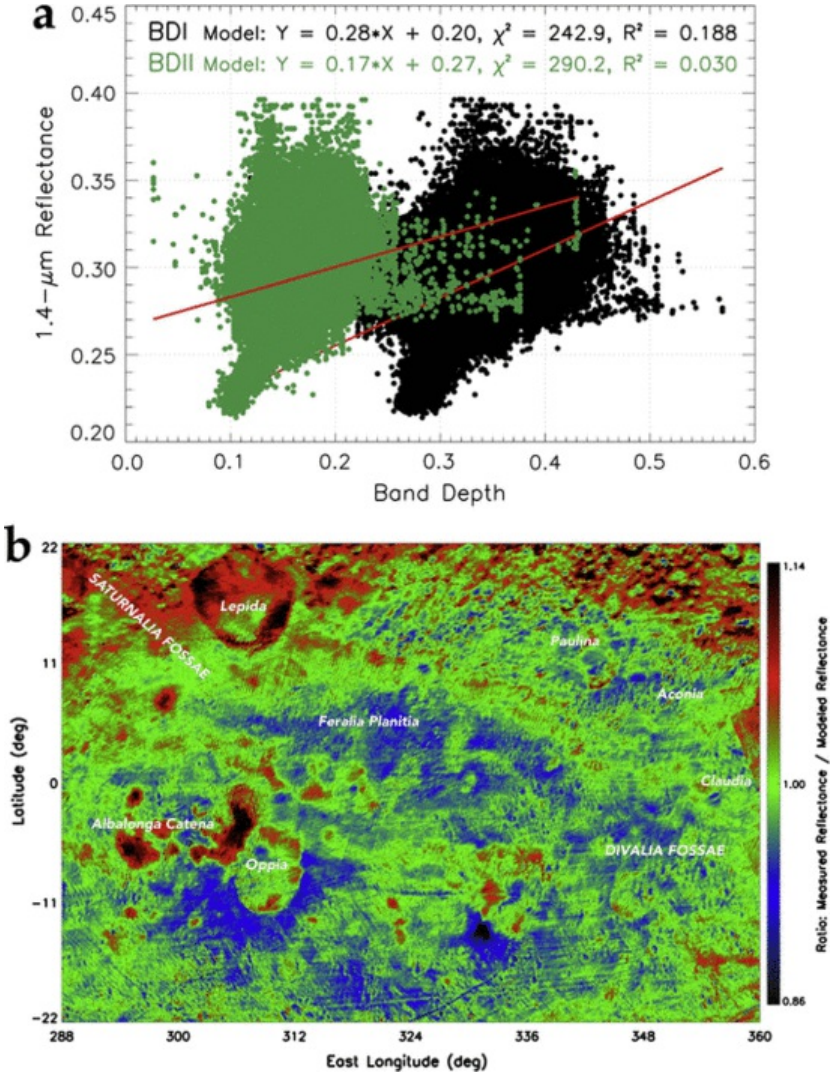

Fig. (If needed, I have the high-resolution (1200 dpi) version of this figure. Please contact me to let me have instructions to upload the high-res file.

) 8 Panel a: Scatterplot of 1.4-μm reflectance as a function of BDI (in black) and BDII (in green). A linear fit model (red line) is superimposed on both distributions. Despite the large spread, and the weak (BDI) or absent (BDII) correlation in the linear fit model, some groups of points showing distinct characteristics can be perceived. Panel b: Ratio between the measured 1.4-μm reflectance and the BDII/1.4-μm linear fit model. This map shows where the surface material significantly departs from the linear correlation. Dark blue to blue colors mark locations that have shallower BDII than average units of the same reflectance, or locations that have reflectance lower than the average value of units with the same BDII. Red to dark red shades mark locations that have larger BDII than average units of the same reflectance, or that have higher reflectance than average units with the same BDII. If BDII was perfectly correlated with the 1.4-μm reflectance, this map would appear uniformly green. (For interpretation of the references to color in this figure legend, the reader is referred to the web version of this article.)

4.4 1.4-µm reflectance and 2.8-µm band depth

The next tool used in our analysis is a comparison between two maps derived from VIR infrared data: the 1.4-µm reflectance map the 2.8-µm band depth map, shown in Fig. 9.

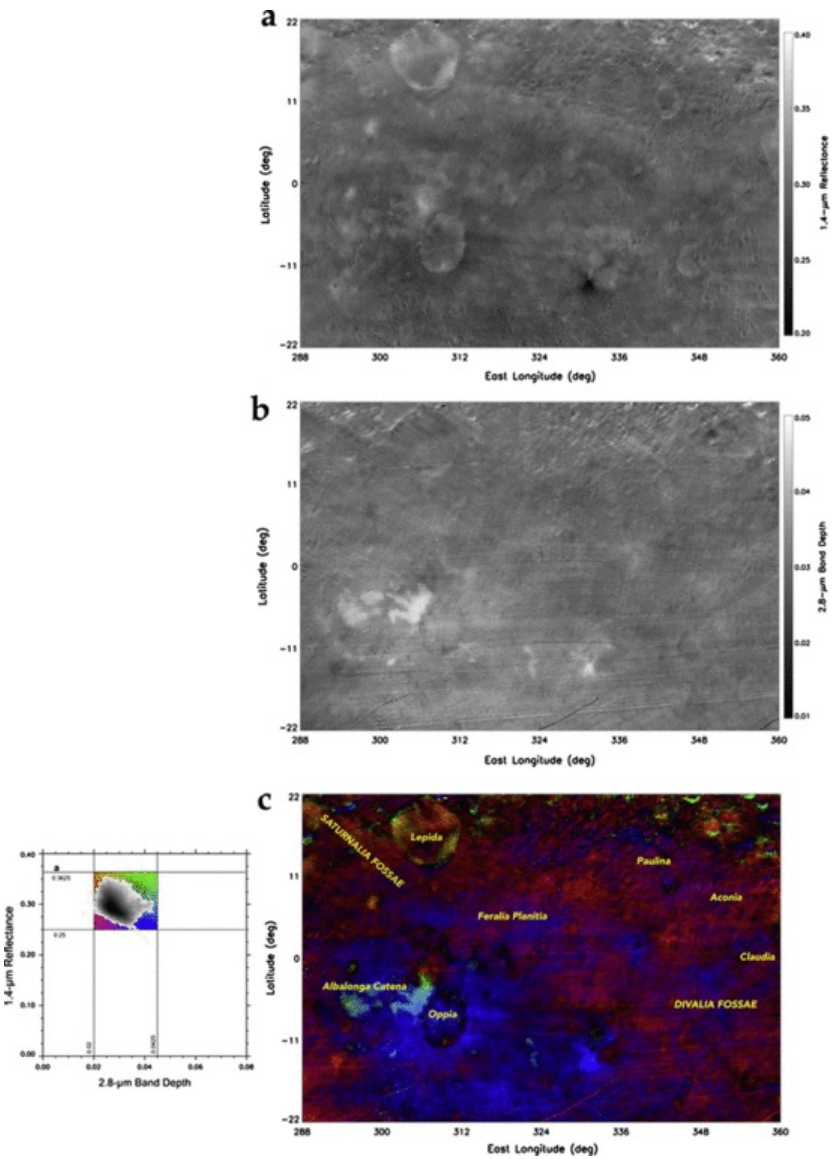

Fig. (Please enlarge Fig. 9 so as it uses the full page.

) 9 P (If needed, I have the high-resolution (1200 dpi) version of this figure. Please contact me to let me have instructions to upload the high-res file.

anel a: Reflectance map of the Av-10 Oppia quadrangle, shown at 1.4 µm, after photometric correction by means of the Akimov disk function. The 5-km Oppia B crater shows higher reflectance, which correlates with higher pyroxene band depths (see Fig. 7). Panel b: Distribution of hydrous materials in the Oppia quad, as traced by the depth of the 2.8-µm absorption signature. On Vesta, hydrated phases are generally correlated with low-reflectance material that has shallow pyroxene bands. However, the ejecta blanket to the west of Oppia represents a notable exception, being significantly enriched in hydrous materials while showing a moderate reflectance. Panel c: Four-color composite map of the Av-10 Oppia quadrangle, showing both 1.4-µm reflectance and 2.8-µm band depth. The 2-D scatterplot on the left serves as color key and legend for the map: anhydrous

compounds appear in purple–red–orange colors, while hydrous compounds are blue–cyan–green. A distinction can be drawn between hydrous minerals showing up in the dark mantle material, displayed in blue, and the OH-rich minerals that characterize the moderate-reflectance light mantle material west of Oppia, which are highlighted in cyan and green. (For interpretation of the references to color in this figure legend, the reader is referred to the web version of this article.)

The appearance of the VIR 1.4-μm reflectance image (Fig. 9a) is consistent with the FC reflectance map: at the VIR spatial resolution (200 m/pixel), the major features of the quadrangle can still be recognized. These include the main deposits of bright and dark materials, such as the dark material originating from the unnamed crater in the lower central portion of the quadrangle and patches of bright material distributed at various other locations, particularly in the ejecta blanket north and west of Oppia. From inspection of Fig. 9b, it appears that the highest concentration of hydrous materials is associated with the ejecta blanket west of Oppia and with the dark material unit. This characteristic distinguishes the Av-10 quadrangle from other places on Vesta, where OH-rich materials associated with dark or very dark material deposits are thought to have been emplaced by the impact of carbonaceous asteroids (De Sanctis et al., 2012b; McCord et al., 2012; Palomba et al., 2014). However, in the Oppia quadrangle, the strongest OH absorptions are found in material with moderate reflectance, most notably the western and northwestern ejecta blanket of Oppia having average VIS reflectance of 0.319 and average 1.4-μm reflectance of 0.296. In Vesta's global mosaic of VIR 2.8-μm band strength, this exception was initially reported by De Sanctis et al. (2012b), although those authors did not provide any detailed description of the distribution of the OH at the local scale in the Oppia region. The hydrous deposits have distinct margins that match the boundaries of light mantle material seen in high-resolution FC imagery. However, not all the light mantle units have OH-bearing materials. The strongest 2.8-μm band depths are concentrated around Oppia in the southwestern portion of the Av-10 quadrangle, whereas light mantle units distributed in the rest of the quadrangle show no OH enhancement. The 2.8-μm band depth in the moderate-reflectance, light mantle units associated with Oppia is as high as 5%. This exceeds the maximum 2.8-μm BD value found in the northern hemisphere of Vesta, which is 4% on a regional scale (De Sanctis et al., 2012b).

The two VIR maps, 1.4-μm reflectance and 2.8-μm band depth, can be conveniently combined into a single color composite map, shown in Fig. 9c, where the color code is designed specifically to take advantage of this information simultaneously. The key to reading this map is provided in the associated legend: the four-color palette is such that dark hydrous materials are blue, bright hydrous materials are green, dark anhydrous materials are red and bright anhydrous materials are orange. This map reveals that all of the Oppia ejecta, including the prominent, spectrally distinct ejecta which are dark orange/red in the Clementine map and have a eucritic composition, show a level of hydration that becomes maximum in the cyan and green ejecta blanket west of Oppia. In contrast, the rest of the quadrangle, which is howarditic in composition, shows reddish tones that do not reveal any trace of hydration, while orange shades are especially indicative of local variations in reflectance, rather than in the degree of hydration.

Fig. 10 presents close-ups of the Oppia crater region, useful for a detailed analysis of the features of interest seen here. In this case, the different panels respectively account for the FC reflectance, Clementine colors, streng~~h~~th of 2.8-μm band, and topography. Focusing on the Oppia ejecta, from previous Fig. 9c one can note a gradient of shades ranging from blue to green, with green (brighter OH-rich material) corresponding to the primary ejecta of the Oppia B crater. Fig. 10d indicates that this area is located at a roughly ~~constant~~uniform elevation (vertical deviations not exceeding 500 m). From Fig. 10b, this Oppia B ejecta has a bright yellow color, distinct from the orange color that characterizes the light mantle material. Moreover, it has much greater BDI and BDII values (Fig. 7) than the rest of the Oppia ejecta. Fig. 10c reveals that here the 2.8-μm BD is 4%, which corresponds to the maximum observed on Vesta on a regional scale (De Sanctis et al., 2012b). However, the western and northwestern rims of Oppia reach the highest values of 2.8-μm BD, which go up to 5% and are comparable with that of the dark crater-ray material in the south-center of the quadrangle (Fig. 9b). Other light mantle (light orange) units with distinct margins, located in the vicinity of the crater both to the north and towards the southeast (the latter is superimposed to the dark mantle material), have a lower OH content. However, they show a substantial contrast in the 2.8-μm BD map and hence reveal an abundance of hydrous minerals greater than the dark mantle material. Conversely, the bright material exposed on the eastern and southern walls of Oppia, which has enhanced pyroxene absorption bands, shows OH band strengths comparable to the average of the quadrangle.

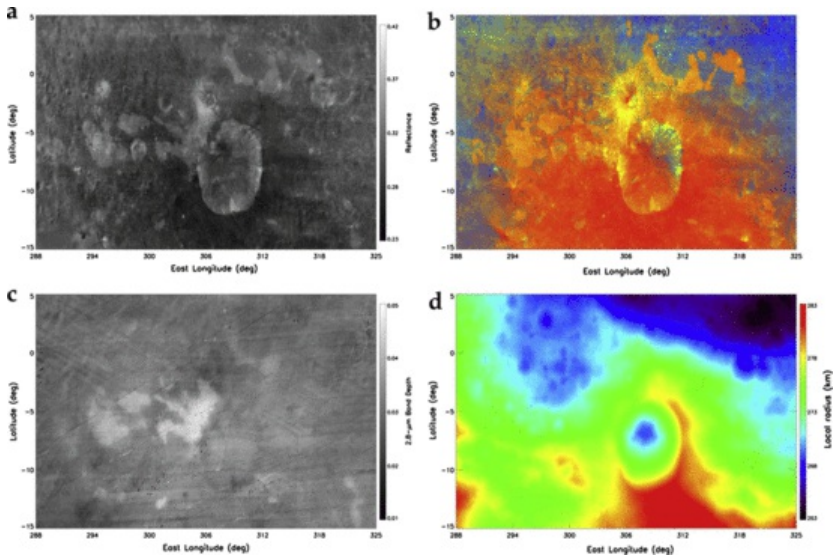

Fig. (If needed, I have the high-resolution (1200 dpi) version of this figure. Please contact me to let me have instructions to upload the high-res file.

10 Close-up of the Oppia crater area covering lat 15°S–5°N and lon 288–325°E. The various panels respectively show: the corrected FC visual reflectance (panel a), the Clementine color ratio map (panel b), the 2.8-μm BD map (panel c) and the topographic map (panel d). The largest abundance of hydrous species is found in the ejecta blanket that match the light mantle material west of Oppia, located roughly at the same elevation. Other light mantle units with distinct margins, located to the north and southeast of the crater, are characterized by lower OH abundances, however greater than the dark mantle material. (For interpretation of the references to color in this figure legend, the reader is referred to the web version of this article.)

From this result, it is possible to go back to VIR spectra to check the possible existence of a spectral signature at 3 μm, linked to the presence of the water molecule adsorbed in surface minerals showing at the same time, the highest strength of the 2.8-μm OH feature. As briefly mentioned in Section 3.1, VIR data acquired at Vesta have substantial calibration residuals in the 3.0–3.1 μm range. However, VIR data acquired in the early Survey phase, although with a lower spatial resolution, do not have this drawback and can be used for this purpose.

Fig. 11 illustrates the difference between the Oppia OH-rich unit west ejecta blanket and a non-hydrated unit at the north of the crater. The data refer to the VIR cube: 366905030, acquired during the Survey phase at a spatial resolution of 0.68 km/px. The spectral ratio shows a broad and very asymmetric absorption band, which suggests multiple absorption processes due to OH-cation bonds, and possibly H–O–H absorptions. The amplitude of the random noise is reduced to about 1% from averaging hundreds of pixels, while the broad and asymmetric absorption band revealed by the ratio reaches 5% amplitude, which rules out the possibility of substantial calibration errors. This spectral feature is much more complex than the hydroxyl absorption band at 2.8-μm commonly found on Vesta. As a consequence, hydrated materials in western Oppia ejecta blankets differ from carbonaceous-chondrite materials. Because the first overtones of the OH stretches occur at about 1.4 μm and the combinations of the H–O–H bend with the OH stretches are found near 1.9 μm (Clark, 1999), to unambiguously prove the existence of water molecules an absorption at 1.9 μm should be seen, which does not yet clearly show up in VIR spectra.

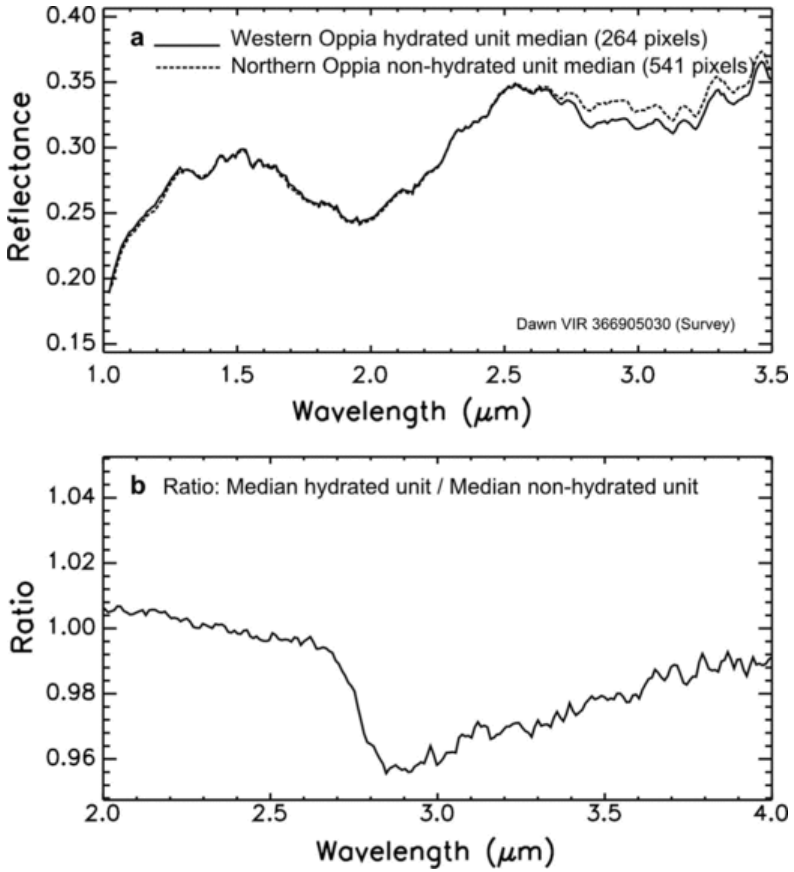

Fig. 11 Panel a: Comparison of spectral profiles between the OH-rich west ejecta blanket of Oppia crater (solid line), and an area to the north essentially devoid of hydrous minerals (dashed line), in the infrared range between 1.0 and 3.5 μm (on the dayside of Vesta, the thermal emission usually shows up longward of ~3.5 μm). The data refer to the VIR cube: 366905030, acquired during the Survey phase at a spatial resolution of 0.68 km/px. The spectrum of the OH-rich region overall shows a deeper absorption in the region between 2.8 and 3.1 μm. Panel b: Ratio between the two

spectra shown in panel a. The spectral ratio clearly displays a broad and very asymmetric absorption band, which differs from the spectra of most hydrous materials found on Vesta and suggests multiple absorption processes. The amplitude of the random noise is reduced to about 1% from averaging hundreds of pixels, while the broad and asymmetric absorption band revealed by the ratio reaches 5% amplitude.

Plotting the values of 1.4-µm reflectance ~~versus~~, 2.8-µm band depth is a good way to explore the correlation between these two parameters (Fig. 12a). The scatterplot reveals a general tendency for 2.8-µm BD to increase with decreasing 1.4-µm reflectance, although the dispersion is so high as not to allow a strong correlation. However, a linear 'tail' of pixels in the lower right portion of the scatterplot in Fig. 12a has low reflectance and 2.8-µm band depths of ~5%. This tail corresponds to the dark crater ray material that is observed in the southern half of the quadrangle. The other concentration of points reaching maximum 2.8-µm BD values of 5% corresponds to the moderate reflectance material concentrated in Oppia's western ejecta blanket.

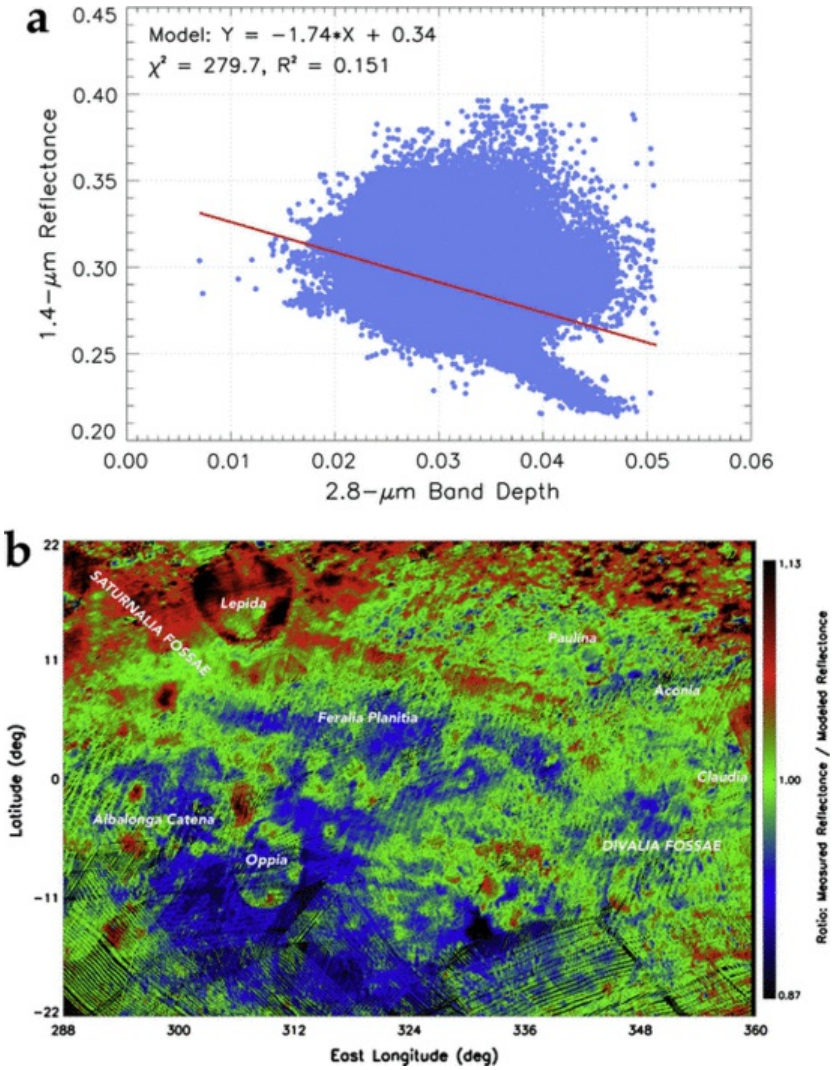

Fig. (If needed, I have the high-resolution (1200 dpi) version of this figure. Please contact me to let me have instructions to upload the high-res file.

) 12 Panel a: Photometrically corrected 1.4-µm reflectance as a function of hydroxyl 2.8-µm absorption band depth for quadrangle Av-10 Oppia, with a model linear fit overplotted (red line). Despite the large spread and the weak anti-correlation, some trends can be seen; most notably the existence of two categories of OH-bearing minerals: one with low reflectance and one with moderate reflectance. Panel b: Ratio between the measured 1.4-µm reflectance and the 1.4-µm/2.8-µm linear fit model. This map shows where the surface material departs substantially from the linear correlation. Dark blue to blue shades indicate materials that are less hydrated than average units of the same reflectance, or materials that have lower reflectance than average units that have the same amount of hydroxyl. Red to dark red tones indicate materials that have larger amount of hydroxyl than average

units of the same reflectance, or that have higher reflectance than average units that have the same amount of hydroxyl. If the 1.4-μm reflectance was perfectly anti-correlated with the hydroxyl absorption band depth at 2.8 μm, this map would appear uniformly green. (For interpretation of the references to color in this figure legend, the reader is referred to the web version of this article.)

The ratio between the measured reflectance and the reflectance modeled by the linear fit is mapped within the quadrangle in Fig. 12b, where blue ~~and green~~ colors correspond to trends significantly lower than the linear one, while ~~the yellow and~~ red tones correspond to trends significantly greater. The majority of the Av-10 quadrangle, showing eucritic mineralogy and including the prominent southern Oppia ejecta, Feralia Planitia and Divalia Fossae, corresponds to the first case, while the northern portion with howarditic mineralogy, including Saturnalia Fossae and the crater Lepida, corresponds to the second case. This is very similar to the map of measured 1.4-μm reflectance vs. BDII/1.4-μm linear fit model seen in Fig. 8b. However, an important exception is the Oppia ejecta that extend to the west and northwest towards Albalonga Catena, which represent important counterexamples to the first case, having reflectance much greater than what is found on average for materials with this abundance of hydrous species.

4.5 Linear spectral unmixing

Fig. 13 displays the result obtained by applying the linear spectral unmixing technique described in Section 3.4 on a limited portion of the surface that includes the crater Oppia. This figure is arranged in several panels that show how VIR data can be conveniently superimposed on higher resolution FC data, in the present case a shaded relief map of the same region, to enable the spectral parameters to be visualized in their three-dimensional context.

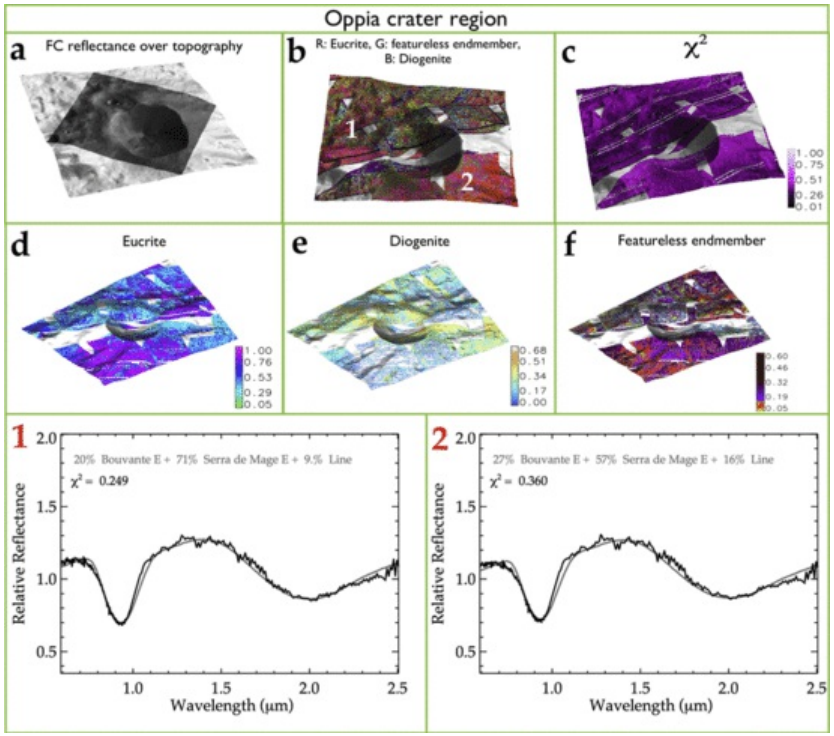

Fig. (If needed, I have the high-resolution (1200 dpi) version of this figure. Please contact me to let me have instructions to upload the high-res file.

13 Result of linear spectral unmixing applied to the crater Oppia region. From top to bottom and from left to right, the panels show respectively: (a) the reflectance derived from FC data in the clear filter (dark gray layer), superimposed to the shape model of Vesta (light gray layer), (b) a RGB color composite that shows the result of the spectral unmixing technique, where the red color marks eucrite, green marks the spectrally flat component and blue marks diogenite; (c) a map of chi-square; and: (d–f) three separate maps that respectively display the relative abundances of eucrite, diogenite, and featureless component (for each pixel, the sum of these abundances is equal to 1). Finally, bottom panels 1 and 2 show examples of linear spectral fit obtained in regions 1 (west ejecta blanket) and 2 (dark mantle material), marked in the white color in panel b. In these plots, the black line represents VIR measured data while the gray line is the best fit. Values of the relative abundance of the three endmembers providing the best fit are specified along with the chi-square value ("line" stands for the spectrally flat component). (For interpretation of the references to color in this figure legend, the reader is referred to the web version of this article.)

The three endmembers that provide a best fit to VIR data are: eucrite, diogenite and the spectrally flat component. However, as mentioned in Section 4.1, pure diogenite is not found within the Oppia quadrangle, so the relative abundance of this endmember is always small when compared to that of eucrite.

The RGB endmember abundance image (Fig. 13b) accounts for the main lithologies, with red corresponding to the abundance of eucrite, green assigned to the featureless component, and blue being diogenite. The relative abundances of these three spectral endmembers are shown separately in Fig. 13d–f. With a high confidence level (chi square < 1, Fig. 13c), the spectral unmixing again confirms that the Oppia ejecta extending to the south, and particularly to the southeast, has a markedly eucritic lithology with varying abundance of the featureless (dark/carbonaceous) material. Finally, bottom panels 1 and 2 display examples of linear spectral fits obtained in two regions highlighted in Fig. 13b: (1) the west ejecta blanket, and (2) the dark mantle material to the southeast. In both cases, best fits are achieved with a eucritic composition and a variable percentage of neutral component, which is higher in the dark mantle material. The eucrite spectral endmembers that provide a best match with VIR data, in decreasing order of frequency, are: Bouvante, Cachari and Serra de Mage (see Zambon et al., submitted~~in preparation~~ for more details about these meteorite samples). The rim of the Oppia crater, including the inner walls close to the rim, and the northern terrain, show an increasing relative abundance of diogenite, thereby representing a transition from eucritic to howarditic mineralogy. The west and northwest ejecta blanket, that is, areas corresponding to light mantle material with enhanced abundance of OH-bearing phases, also have a eucritic composition, although in lesser proportions than that found in the southeastern ejecta.

4.6 Surface temperature

In the case of the Oppia quadrangle we have considered only surface temperature data retrieved from VIR infrared observations obtained in the HAMO and HAMO-2 phases, in order to maintain uniformity in both the pixel resolution and the local solar time (the majority of the observations acquired in these two phases of the mission took place in the vestan morning). For this reason, there are major gaps in coverage compared to other VIR maps shown previously, as revealed by Fig. 14. The surface temperature map is accompanied by a map of the solar incidence angle, so as to allow a comparison with the instantaneous solar illumination.

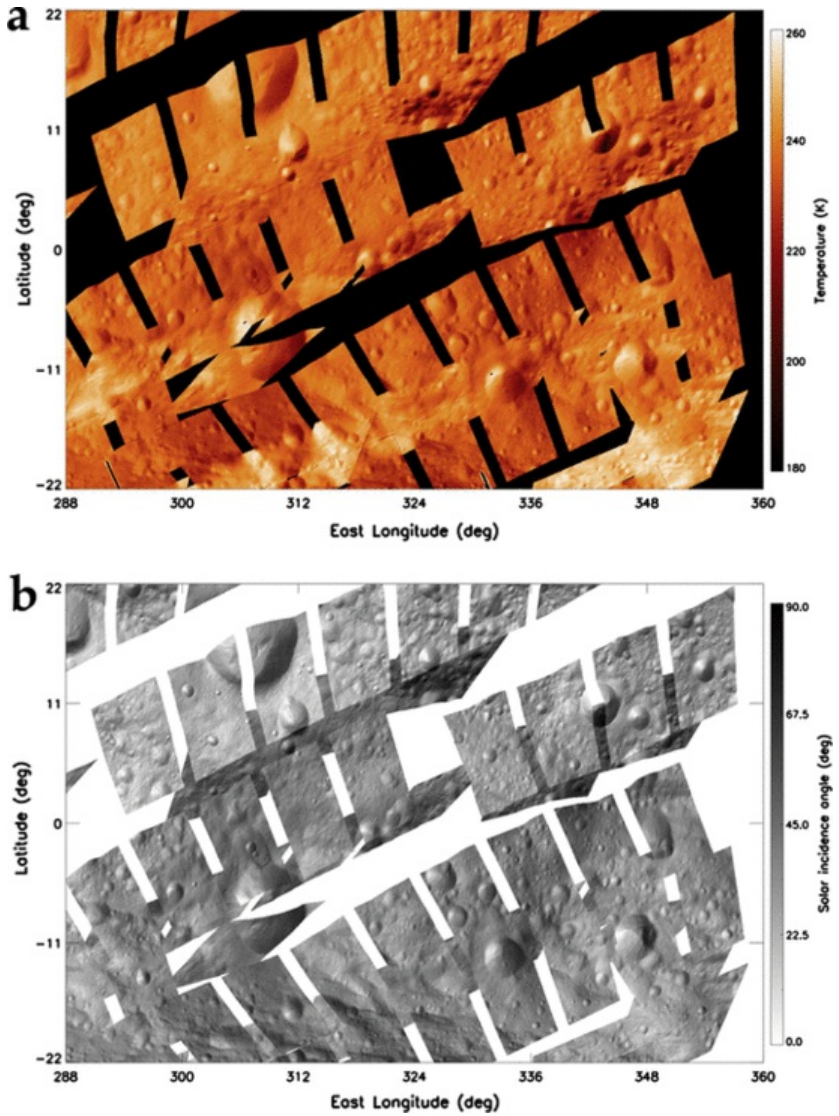

Fig. (If needed, I have the high-resolution (1200 dpi) version of this figure. Please contact me to let me have instructions to upload the high-res file.

) 14 Panel a: Surface temperature map of quadrangle Av-10 Oppia, derived from VIR infrared data acquired in the HAMO and HAMO-2 phases at an average resolution of 0.18 km/px and in the vestan morning. A "red temperature" color bar is adopted, such that coldest temperatures are shown in the dark red tones while warmest temperatures are whitish. The lower limit (180 K) is set by the VIR sensitivity range and the rms level of in-flight noise. In the range of local solar times analyzed here, surface temperatures are as high as 260 K. Panel b: Solar incidence angle map of the same region. Surface temperatures recorded in panel a generally follow the local topography, in such a way that areas illuminated at large incidence angles (dark tones) are cooler than materials illuminated at small incidence angles (bright tones). (For interpretation of the references to color in this figure legend, the reader is referred to the web version of this article.)

To first order, the map shows no macroscopic evidence for major inhomogeneities in temperature: thermal shades in the top panel can generally be explained by solar illumination combined with the local topography at the time of the observations. As discussed in the previous sub-sections, the crater Oppia is peculiar in many respects, yet it does not show any significant thermal anomaly, due to differences in albedo (associated with possible differences in emissivity) or to differences in local density. This suggests that, at least to the degree that can be determined by VIR, the thickness of the regolith in the Av-10 quadrangle overall is large enough to mask any inhomogeneity in the density and/or thermal conductivity of surface material. In contrast, other Vesta

quadrangles contain examples of bright material units often characterized by detectable thermal differences compared to surrounding terrains (Tosi et al., 2014; Zambon et al., this issue), or the occasional presence of distinct thermal behaviors associated with specific geological features (e.g., Denevi et al., 2012; Stephan et al., 2014~~, this issue~~; McFadden et al., this issue).

Both the prominent ejecta associated with Oppia's dark mantle material and the OH-rich west ejecta blanket do not show thermal behavior consistent with a different compactness of the surface material. Oppia B, with its exposure of bright material, does not display a decrease in temperature unrelated to local topography. The dark crater ray material in the lower half of the quadrangle does not show any detectable difference in temperature, compared to the surrounding terrains observed under similar conditions of solar illumination and local solar time. This is consistent with the weak correlation that on Vesta is generally observed in the temperature of dark material units as a function of albedo (Tosi et al., 2014).

5 Main geologic units of Av-10 and Oppia crater region

To investigate the properties of the medium-scale geologic units and fit them properly in the context of the general mineralogy of the Av-10 quadrangle, we consider twelve regions of interest, also partly discussed in the geologic mapping paper of this same quadrangle (Garry et al., 2014): (1) light mantle material west of Oppia, (2) light mantle material north of Oppia, (3) dark mantle material south of Oppia; (4) Lepida crater; (5) Oppia crater; (6) Paulina crater; (7) Saturnalia Fossae; (8) Feralia Planitia; (9) heavily cratered highlands; (10) Divalia Fossae; (11) Oppia B crater; (12) unnamed crater with dark material at 12.5°S, 333.7°E. For each of these features, we computed the mean value and standard deviation of the spectral parameters used in this work: BCI, BCII, BDI, BDII, VIS reflectance, 1.4-μm reflectance, and 2.8-μm BD. These values are summarized in Table 1. We intentionally do not report the minimum and maximum values of each spectral parameter, because they represent extreme cases of a distribution of points that can easily overlap between different features, confounding the interpretation. In contrast, mean and standard deviation are indicative of the behavior of the majority of the data.

Table 1 Summary of the statistics computed for the spectral parameters of the main geologic features in Av-10 quad. In each column, the bold and bolditalic respectively mark the minimum and maximum values recorded for a given spectral parameter.

		BCI	BCII	BDI	BDII	VIS refl.	1.4-μm refl.	2.8-μm BD
Oppia's light mantle W	Mean	0.9265	1.9777	0.3566	0.1722	0.3193	0.2954	***0.0393***
	Stdev	0.0023	0.0065	0.0227	0.0159	0.0154	0.0103	0.0038
Oppia's light mantle N	Mean	0.9263	1.9799	0.3466	0.1692	***0.3264***	0.2954	0.0317
	Stdev	0.0015	0.0054	0.0138	0.0099	0.0103	0.0067	0.0024
Oppia's dark mantle S	Mean	0.9265	***1.9908***	0.3232	0.1582	**0.2762**	0.2766	0.0326
	Stdev	0.0025	0.0067	0.0125	0.0106	0.0112	0.0071	0.0021
Crater Lepida	Mean	0.9265	1.9712	0.3523	0.1585	0.3255	***0.3129***	**0.0281**
	Stdev	0.0016	0.0059	0.0175	0.0101	0.0159	0.0133	0.0021
Crater Oppia	Mean	0.9252	1.9831	0.3410	0.1713	0.3034	0.2874	0.0337
	Stdev	0.0024	0.0097	0.0238	0.0160	0.0181	0.0099	0.0024
Crater Paulina	Mean	0.9252	1.9708	0.3449	0.1531	0.3175	0.2931	0.0288
	Stdev	0.0019	0.0059	0.0207	0.0145	0.0141	0.0099	0.0018
Saturnalia Fossae	Mean	0.9264	1.9711	0.3430	0.1504	0.3259	0.3105	0.0283
	Stdev	0.0019	0.0042	0.0263	0.0119	0.0144	0.0104	0.0026
Feralia Planitia	Mean	0.9257	1.9836	**0.3223**	0.1507	0.3094	0.2852	0.0285
	Stdev	0.0016	0.0062	0.0164	0.0100	0.0123	0.0064	0.0018
Heavily cratered highlands	Mean	**0.9249**	**1.9685**	0.3444	0.1547	0.3159	0.2981	0.0283
	Stdev	0.0019	0.0069	0.0232	0.0139	0.0142	0.0124	0.0023

Divalia Fossae	Mean	0.9263	1.9812	0.3290	0.1518	0.3126	0.2899	0.0285
	Stdev	0.0021	0.0058	0.0136	0.0091	0.0127	0.0074	0.0018
Oppia B	Mean	***0.9267***	1.9794	***0.3709***	***0.2019***	0.3213	0.3097	0.0293
	Stdev	0.0016	0.0064	0.0217	0.0136	0.0199	0.0127	0.0035
Unnamed crater with dark material	Mean	0.9263	1.9825	0.3223	**0.1471**	0.3010	**0.2812**	0.0329
	Stdev	0.0023	0.0062	0.0212	0.0136	0.0257	0.0180	0.0032

Inspection of Table 1 allows us to quickly identify, for each spectral parameter, the highest and lowest average value among all considered geologic features. First, it is possible to observe how the values of BCI are actually confined to a very narrow range, which makes this parameter less useful than BCII for the discrimination of mineralogy in these regions of interest. Some geologic features clearly stand out: for example, cratered highlands in the far northeast have the lowest values of BCI and BCII, and therefore, as inferred from the general map, have a distinctly howarditic composition (including a few sites where diogenite-rich howardite is found). For comparison, the Oppia ejecta are definitely eucritic, but the table shows that the dark mantle material (dark orange/red) that extends to the south and has a relatively low VIS reflectance, is by far the most eucritic in Av-10.

Examining the band depth, both Feralia Planitia and the unnamed crater with dark material show the minimum values of BDI. This same crater also has low values of both VIS and NIR reflectance and BDII, in agreement with what is generally observed for dark and very dark material units on Vesta (Palomba et al., 2014). Conversely, the highest BD values are recorded for Oppia B. However, this is not the brightest feature of the entire quadrangle. Light mantle material north of Oppia and Saturnalia Fossae, on average, have a higher reflectance in the VIS (FC map). On the other hand, the brightest geologic features in the NIR (1.4-μm) are crater Lepida and Saturnalia Fossae in the far northwest, because of the presence of several bright material units in that area. Finally, light mantle material west of Oppia is by far the richest in OH-bearing material, whereas the areas showing the weakest OH band are the crater Lepida, the cratered highlands, and the Saturnalia Fossae. Craters Oppia and Paulina, as well as Divalia Fossae, have similar characteristics and do not hold any substantially high or low value of any of the spectral parameters considered here, except for the content of hydrous minerals, which is definitely more enhanced in Oppia crater.

Near Oppia, the crater density does not relate with albedo or color variations. This seems to be caused by individual resurfacing processes at different sites. While this affects the determination of local surface ages by crater counting, a more plausible age determination or at least the determination of the succession of deposition or exposure of specific color units is better constrained by a geologic and morphologic context study. Craddock and Howard (2000) looked at degradation of individual craters on the Moon. Their method can be expanded by comparing the shapes and borders of areas showing different colors, or by evidence from geology (e.g., landslides that may show up in craters, with one material on top of another), highlighting the succession of deposition. Unfortunately, different features may not show a consistent scenario: at the borders of orange material and usual howarditic material, deformation by resurfacing is observed, indicating opposite successions. This is an indication of a complex evolution of this region.

The level of detail offered by FC imagery proves very valuable when considering color ratios alternative to the classic Clementine presentation, which can highlight new differences or otherwise hidden textures. Fig. 15a is a close-up of the Oppia crater region seen in the FC clear filter, with numbers and roughly sketched boundaries that mark different surface units. Fig. 15b is a color composite image of Oppia, obtained with color ratios alternative to the Clementine ratio: R = 0.44-μm × (0.65-μm/0.55-μm); G = 0.83-μm × (0.96-μm/0.92-μm); B = 0.75-μm × (0.92-μm/0.83-μm). Fig. 15c reveals high-resolution details of the northern part of Oppia crater, acquired in the clear filter during the LAMO mission phase. Finally, Fig. 15d shows a comparison between FC spectra of the 10 surface units identified in Fig. 15a, plus two spectra (dashed lines) of the orange ejecta of Octavia crater in the quadrangle Av-8 (Marcia).

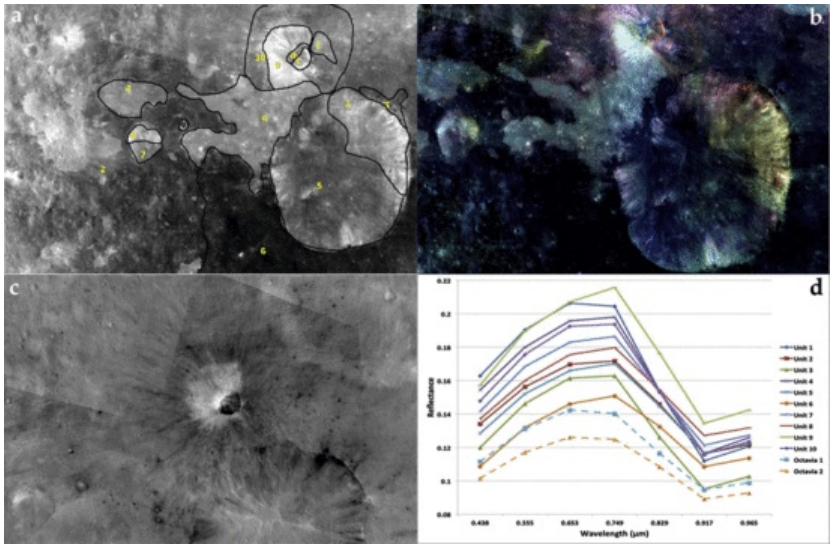

Fig. (If needed, I have the high-resolution (1200 dpi) version of this figure. Please contact me to let me have instructions to upload the high-res file.

) 15 Panel a: Close-up of the Oppia crater region, with numbers and roughly sketched boundaries that mark different surface units. Panel b: Color composite image of Oppia, obtained with color ratios alternative to the Clementine ratio: R = 0.44-μm × (0.65-μm/0.55-μm); G = 0.83-μm × (0.96-μm/0.92-μm); B = 0.75-μm × (0.92-μm/0.83-μm). The color scale is indicative of different compositions and/or different degrees of maturity of the soil. Panel c: Detail of the northern part of Oppia crater, acquired in the FC clear filter during the LAMO mission phase. We note the widespread occurrence of small dark material units, which suggest the presence of a layer of carbonaceous chondrite material older than Oppia. Panel d: FC spectra of the 10 surface units identified in panel a (solid lines), plus two spectra (dashed lines) of the orange ejecta of Octavia crater in the quadrangle Av-8 (Marcia). (For interpretation of the references to color in this figure legend, the reader is referred to the web version of this article.)

Under the assumption that equal pseudo-colors shown in Fig. 15b roughly correspond to a similar degree of maturity (age) of the terrains, we can distinguish at least five local-scale homogeneous surface units: (a) material representative of the original crust; (b) a layer with dark carbonaceous chondrite (CC) material; (c) a subsequent layer of moderate reflectance, lobated material (light mantle material), followed by (d) the impact that generated Oppia and its major ejecta, and finally (e) a significant alteration provided by the Oppia B crater.

In a tentative chronological order from older to younger, we give a brief description of the areas tagged in Fig. 15a:

1. Old eucritic/howarditic crustal material, now freshly exposed. Its spectrum is close to the average Vesta spectrum, except it is slightly more eucritic.
2. Gardened surface after inclusion of diffuse, dark CC material from the northern hemisphere of Vesta (De Sanctis et al., 2012b; McCord et al., 2012) and the 'dark ribbon' feature (a long runout ejecta flow that cuts across nearby quadrangle Av-9 'Numisia', see Buczkowski et al., 2014; Frigeri et al., this issue-b). Its reflectance is lower than average and has a shallower band I.
3. Area with scattered higher concentration of CC material, mostly freshly exposed by impacts. From VIR data, it appears de-hydrated and possibly metamorphosed. Its reflectance is lower than (2) and its visible spectral slope is higher than (2).
4. Coating by lobate, light mantle material. It has a substantially red visual slope, moderately deep band I, slightly lower reflectance than the fresh exposure of old material (1), and shows the highest level of hydration as measured by VIR.
5. Mixture of original and projectile material inside Oppia. Its reflectance is intermediate between the original Vesta crust (1) and the main ejecta (6). Its visible spectral slope is also higher than (2).
6. Oppia's main ejecta, mapped as dark mantle material. They have the lowest reflectance and the highest visible spectral slope. This material has a markedly eucritic mineralogy and a moderate hydration, and perhaps retains a greater proportion of projectile components.
7. Slumped sheet from materials (2) and (4) into a crater which otherwise exposes material type (4). It has a substantial degree of hydration and is similar than (2), but is brighter and redder.
8. Unique material at the center of Oppia B, similar to the center of Aelia crater. It is darker and redder than (4), but has a deeper band I. Its spectral profile as measured by FC best matches with a small component of HED impact melt.
9. Primary ejecta of Oppia B. They are substantially bright, and similar in spectral shape to (8). They might result from a mixture of fine grained material, with older background material completely blanketed.
10. Region of ejecta rays from Oppia and transition to background material. Darker than (9), with a deeper band I.

6 Discussion and conclusions

Av-10 Oppia is one of the most interesting quadrangles in the Vesta's equatorial region, and on the asteroid in general. In this work we have undertaken a thorough investigation of the mineralogy of the Oppia quadrangle, using various techniques designed to complement and expand the analysis performed in previous work, providing quantitative results that can be directly compared with those obtained for other vestan quadrangles, which are discussed in this special issue by means of similar techniques.

The southwestern portion of the quadrangle is dominated by the crater Oppia's ejecta, whose spectroscopic characteristics differ strongly from the average of the rest of the asteroid. This contrast is appreciable on a broadly regional scale, enough to be first noticed in ground-based observations (Gaffey, 1997) and later recognized by HST observations (Li et al., 2010). These ejecta extend to the Rheasilvia impact basin and influence a large region that includes the southern quadrangles Urbinia and Tuccia (Kneissl et al., 2014; Zambon et al., this issue). The composition of the Av-10 quadrangle reflects the sequence of events that shaped its geologic history: a densely cratered and therefore ancient region was modified by more recent impacts, especially the one that generated the crater Oppia. The result is an asymmetry that affects the quadrangle, with the northern region, particularly the heavily cratered highlands in the far northeast, showing a howarditic lithology, as opposed to the south-central region, surrounding Oppia crater, which is more eucritic. The absence of diogenite confirms that the range of longitudes sampled by Av-10 is unaffected by ejecta produced by the Rheasilvia and Veneneia south polar basins (De Sanctis et al., 2012a; McSween et al., 2013). If diogenitic ejecta were originally present in this area, most notably in Saturnalia and Divalia whose age is compatible with those events (Williams et al., 2014b), today they are buried or erased by subsequent events that have significantly altered the mineralogy. The few sites in Av-10 where diogenite-rich howardite is found are all located elsewhere, particularly in the heavily cratered highlands in the far northeast, sampling the oldest crust.

The dark orange/red diffuse deposit of southern Oppia ejecta is the most prominent multispectral unit in the global Clementine color ratio mosaic. The origin of this material has been proposed to be a glassy melt-sheet deposited by an impact that occurred on a sloping target area (Le Corre et al., 2013; Garry et al., 2014). Material with these unusual color properties is not observed at older craters with eroded rims, suggesting that the impact melt, if present also in those cases, must have been diluted and mixed with the background regolith over time (Le Corre et al., 2013). However, our investigation shows that the composition of the Oppia ejecta is not homogeneous. VIR data reveal that the highest BCII values (most eucritic material) are recorded in the ejecta deposited to the southeast, an area with correspondingly low values of reflectance and pyroxene band depth. In contrast, the ejecta located to the northwest and west have a composition that grades from eucrite to eucrite-rich howardite, respectively. The Oppia crater itself displays considerable variability in its interior. The floor of the crater is eucritic and shows relatively low values of pyroxene band depth, whereas the rim has higher reflectance, correspondingly larger band depths, and a mineralogy that is locally shifted to the typical range of eucrite-rich howardite.

The most important findings from the mineralogical analysis of quadrangle Av-10 concern the Oppia ejecta corresponding to light mantle material. The deposits closest to Oppia, in particular those concentrated towards the west and northwest, show the highest relative 2.8-μm absorption band depth (up to ~5%) in the entire quadrangle. The strength of the OH signature is comparable to that determined for a dark material unit in a nearby crater, yet does not correspond to any dark material but rather to moderate reflectance material. This association of moderate reflectance with relatively strong 2.8-μm band is a rare occurrence on Vesta, having been detected only in one other case, crater Aelia in the Av-7 Lucaria quadrangle (Longobardo et al., this issue).

According to the initial analysis of Le Corre et al. (2013), all light orange material sites appear compositionally homogeneous in terms of VIR BI and BII characteristics. Our work, which includes analysis of VIR data for the portion of the spectrum near 3 μm, shows that in fact, not all patches of light mantle material within the quadrangle have similar abundance of hydrous species. In moving away from Oppia in the north and east directions, the strength of OH-bearing phases in light mantle material gradually decreases to background levels. Therefore, a given orange tone in the FC-derived Clementine color-ratio composite map does not necessarily correspond to the same composition everywhere. Furthermore, our in-depth analysis shows that the infrared spectrum of the OH-rich material in the west ejecta blanket of Oppia has a hydration feature larger and significantly different than the one usually reported for dark, carbonaceous chondrite material on Vesta, which might suggest the presence of H–O–H absorptions. While we still lack a reliable detection of water in this region, or anywhere on Vesta, this initial result leaves room for extensive investigation with VIR data, acquired at relatively low spatial resolution in the early stages of the orbital mission, to map regional and global trends across the asteroid. In a broader respect, this finding of a compositional difference that does not produce color differences in the extended visible part of the spectrum sensed by FC (~0.4 to 1.0 μm) reinforces the key utility of infrared wavelengths longward of 1 μm. In particular, the 3-μm region sampled by VIR provides additional information on the nature and distribution of the materials present in the surface. The diffuse dark mantle material (dark orange/red) south of Oppia also shows the signature of hydrous minerals, although 2.8-μm band strengths are reduced. The VIR data also reveal the presence of OH-bearing phases in the Feralia Planitia basin, whereas the northern and northeastern sections of Av-10, i.e., those with predominantly howarditic mineralogy, are essentially anhydrous.

In Vesta quadrangle Av-8 (Marcia), the orange ejecta of the Octavia crater have a eucritic mineralogy, similar to what is observed for the dark mantle material in Oppia. Octavia shows the same kind of features seen in the detailed close-up of Oppia, but is generally darker, which reveals a higher concentration of carbonaceous components, even though OH concentrations are lower than the light mantle unit west of Oppia (De Sanctis et al., this issue). One could therefore hypothesize that these Oppia and Octavia terrains have a common nature. In principle, their positive spectral slope in the visible could result from a variety of metal–silicate mixtures that induce weaker absorption bands and lower albedo compared to pure pyroxenes. However, Le Corre et al. (2013) demonstrated that the visible slope of orange deposits on Vesta, as measured by the FC 0.75-μm/0.44-μm reflectance ratio, is overall incompatible with mixtures of metals and silicate. We can also rule out that the peculiarity of the Oppia terrain is somehow related to substantial heterogeneity in the grain size. A scatterplot of BDII vs. 1.4-μm reflectance shows in fact that the OH-rich orange material west of Oppia has

a very homogeneous grain size, consistent with the typical values found across much broader regions on Vesta (<45 μm).

Differences in materials with a positive spectral slope have been found in other places on Vesta. For example, orange materials in the Av-6 Gegania quadrangle are relatively bright and howarditic, while those of Lucaria are darker and eucritic (Schäfer et al., 2014; Longobardo et al., this issue). The explanation provided by those authors is that the former were generated by the Rheasilvia impact event, while the latter were generated by the Octavia impact. Indeed, mapping of the light mantle units in Av-10 suggests that some light mantle deposits could be distal ejecta from Oppia and Octavia, deposited hundreds of kilometers away from the craters due to the low gravity of Vesta (Garry et al., 2014). Therefore, the abundance of OH-bearing minerals may also help in discriminating the origin (age) of some light orange units across the surface: those with low or no OH abundance might be associated with events that occurred at a considerable distance (where the crust was depleted in ~~carbonaceus~~carbonaceous chondrite material), and/or are older and underwent dehydration processes in the space environment for a longer time.

For the Aelia crater in Av-7 (Lucaria) quadrangle, the explanation offered to explain the presence of OH-rich minerals in moderate reflectance material is that dark and bright materials are intimately mixed (Longobardo et al., this issue). It should also be noted that Aelia crater is one of the few examples on Vesta where freshly exposed bright material has a diogenitic composition (Zambon et al., 2014), whereas diogenite is not found in the Oppia crater region. Oppia also lacks prominent bright or dark crater rays extending from the crater rim, while such rays are found at other smaller but clearly fresh impact craters on Vesta (Stephan et al., 2014). The lack of rays could indicate that such features have been erased by impact gardening due to the relatively older age of Oppia compared to craters with distinct ejecta rays (Pieters et al., 2012; Le Corre et al., 2013). Furthermore, a close inspection of Oppia finds that bright slope materials are exposed on the inner walls close to the rim, and the widespread occurrence of small, localized dark material units seen in FC imagery at the highest spatial resolution, including dark crater rays in Oppia B, reveals a layer of dark carbonaceous material existing prior to the Oppia event.

On Vesta it is common to come across impact craters that expose layers of both dark and bright material. The bright layers are thought to correspond to fresh material processed by relatively little space weathering, whereas the low reflectance of the dark material results from delivery of carbonaceous impactors over time (McCord et al., 2012). If the explanation given for Aelia also applies to Oppia, the impact that created Oppia could have affected a portion of Vesta originally rich in hydrated material, penetrating the crust enough to excavate brighter and less-processed material and cause intimate mixing with the dark material, which originally covered the brighter subsurface. The fact that Oppia's eucritic ejecta are overall affected by the OH spectral signature supports this hypothesis. However, it is equally clear that this mixing, if plausible, was more effective in the western region of the crater, where today we still can see the highest abundance of the OH-bearing phase, and we even hint the possible occurrence of H–O–H bonds. It should also be noted that the floor of crater Oppia shows no pitted terrains of the kind found within the Cornelia and Marcia craters. The pits, which are rare on Vesta, are thought to form through degassing of a volatile-rich soil heated by the impact (Denevi et al., 2012). Even the floors of Marcia and Cornelia are rich in hydrous minerals while not showing the signature of water (De Sanctis et al., 2015a).

Although the variety of colors and spectral information that the Dawn mission was able to get in the Oppia quadrangle has disclosed a fascinating world, the synoptic that can be drawn from our work is still far from being able to provide definitive answers to the many open questions concerning the composition and distribution of surface materials in Oppia, and more generally on Vesta. One irrefutable piece of evidence is that the Oppia event substantially changed the mineralogy of the entire quadrangle. We support the hypothesis, already advanced for other similar cases, that the hydrous material with substantial positive visible slope that is seen today in this region is the product of an intimate mixing of bright, unaltered material, representative of the original vestan crust, and a layer rich in hydrated minerals. This result may have been favored by both the pre-existing mineralogy and the characteristics of the impact event. In addition, space weathering processes might have dehydrated surface materials of the light mantle with time, but not enough to erase the footprint of a composition that most likely stood out even in earlier times.

Acknowledgments

This work was supported by the Italian Space Agency (ASI), ASI-INAF Contract I/004/12/0. The authors thank the Dawn Science, Operation and Instrument Teams for a successful Dawn at Vesta mission. D.T. Blewett received support from the NASA Dawn at Vesta Participating Scientist program. The VIR instrument was developed under the leadership of INAF, Italy's National Institute for Astrophysics, Rome. The instrument was built by SELEX-Galileo, Florence, Italy. We thank Jennifer Scully and Sharon Uy for their assistance in revising the manuscript. Dawn datasets are publicly available at the Planetary Data System Small Bodies Node (http://pdssbn.astro.umd.edu/).

References

Adams J.B., Visible and near-infrared diffuse reflectance spectra of pyroxenes as applied to remote sensing of solid objects in the Solar System, *J. Geophys. Res.* **79**, 1974, 4829–4836, http://dx.doi.org/10.1029/JB079i032p04829.

Akimov L.A., Influence of mesorelief on the brightness distribution over a planetary disk, *Soviet Astron.* **19** (3), 1975, 385–388, (Astronomicheskii Zhurnal 52, 635–641).

Ammannito E., et al., *Nature* **504** (7478), 2013, 122–125, http://dx.doi.org/10.1038/nature12665.

Binzel R.P., et al., Geologic mapping of Vesta from 1994 Hubble Space Telescope images, *Icarus* **128**, 1997, 95–103, http://dx.doi.org/10.1006/icar.1997.5734.

Buczkowski D.L., et al., The unique geomorphology and physical properties of the Vestalia Terra plateau, *Icarus* **244**, 2014, 89–103, http://dx.doi.org/10.1016/j.icarus.2014.03.035.

Burbine T.H., et al., Vesta, Vestoids, and the howardite, eucrite, diogenite group: Relationships and the origin of spectral differences, *Meteorit. Planet. Sci.* **36** (6), 2001, 761–781, http://dx.doi.org/10.1111/j.1945-5100.2001.tb01915.x.

Burbine T.H., et al., Pyroxene mineralogies of near-Earth vestoids, *Meteorit. Planet. Sci.* **44**, 2009, 1331–1341, http://dx.doi.org/10.1111/j.1945-5100.2009.tb01225.x.

Capria M.T., et al., Vesta surface thermal inertia properties map, *Geophys. Res. Lett.* **41** (5), 2014, 1438–1443, http://dx.doi.org/10.1002/2013GL059026.

Clark R.N., Spectroscopy of rocks and minerals, and principles of spectroscopy, In: Rencz A.N., (Ed), *Manual of Remote Sensing, Remote Sensing for the Earth Sciences* **vol. 3**, 1999, John Wiley & Sons; New York, 3–58, (Chapter 1).

Clark R.N. and Roush T.L., Reflectance spectroscopy – Quantitative analysis techniques for remote sensing applications, *J. Geophys. Res.* **89**, 1984, 6329–6340, http://dx.doi.org/10.1029/JB089iB07p06329.

Cloutis E.A. and Gaffey M.J., Pyroxene spectroscopy revisited – Spectral–compositional correlations and relationship to geothermometry, *J. Geophys. Res.* **96** (E5), 1991, 22809–22826, http://dx.doi.org/10.1029/91JE02512.

Cloutis E.A., et al., The 2.5–5.1 μm reflectance spectra of HED meteorites and their constituent minerals: Implications for Dawn, *Icarus* **225**, 2013, 581–601, http://dx.doi.org/10.1016/j.icarus.2013.04.022.

Combe, J.-Ph. et al., 2015a. Reflectance and hydrated materials of Vesta. Icarus (this issue-a).

Combe, J.-Ph. et al., 2015b. Dawn at Vesta: Composition of the northern regions. Icarus (this issue-b)-. http://dx.doi.org/10.1016/j.icarus.2015.04.026.

Consolmagno G.J. and Drake M.J., Composition and evolution of the eucrite parent body – Evidence from rare Earth elements, *Geochim. Cosmochim. Acta* **41**, 1977, 1271, http://dx.doi.org/10.1016/0016-7037(77)90072-2.

Craddock R.A. and Howard A.D., Simulated degradation of lunar impact craters and a new method for age dating farside mare deposits, *J. Geophys. Res.* **105** (E8), 2000, 20387–20402, http://dx.doi.org/10.1029/1999JE001099.

De Sanctis M.C., et al., The VIR spectrometer, *Space Sci. Rev.* **163** (1–4), 2011, 329–369, http://dx.doi.org/10.1007/s11214-010-9668-5.

De Sanctis M.C., et al., Spectroscopic characterization of mineralogy and its diversity across Vesta, *Science* **336** (6082), 2012a, 697–700, http://dx.doi.org/10.1126/science.1219270.

De Sanctis M.C., et al., Detection of widespread hydrated materials on Vesta by the VIR imaging spectrometer on board the Dawn mission, *Astrophys. J.* **758**, 2012b, L36, http://dx.doi.org/10.1088/2041-8205/758/2/L36.

De Sanctis M.C., et al., Vesta's mineralogical composition as revealed by the Visible and InfraRed spectrometer on Dawn, *Meteorit. Planet. Sci.* **48**, 2013, 2166–2184, http://dx.doi.org/10.1111/maps.12138.

De Sanctis M.C., et al., Mineralogy of Marcia, the youngest large crater of Vesta: Character and distribution of pyroxenes and hydrated material, *Icarus* **248**, 2015a, 392–406, http://dx.doi.org/10.1016/j.icarus.2014.10.051.

De Sanctis, M.C. et al., 2015b. Eucritic crust remnants and the effect of in-falling hydrous carbonaceous chondrites characterizing the composition of Vesta's Marcia region. Icarus (this issue)-. http://dx.doi.org/10.1016/j.icarus.2015.05.014.

Denevi B.W., et al., Pitted terrain on Vesta and implications for the presence of volatiles, *Science* **338** (6104), 2012, 246–249, http://dx.doi.org/10.1126/science.1225374.

Feierberg M.A. and Drake M.J., The meteorite–asteroid connection – The infrared spectra of eucrites, shergottites, and Vesta, *Science* **209**, 1980, 805, http://dx.doi.org/10.1126/science.209.4458.805.

Frigeri, A. et al., 2015a. The spectral parameters maps of Vesta from VIR data. Icarus (this issue-a).

Frigeri, A. et al., 2015b. Mineralogic mapping of the Av-9 Numisia quadrangle of Vesta. Icarus (this issue-b).

Gaffey M.J., Spectral reflectance characteristics of the meteorite classes, *J. Geophys. Res.* **81** (5), 1976, 905–920, http://dx.doi.org/10.1029/JB081i005p00905.

Gaffey M.J., Surface lithologic heterogeneity of Asteroid 4 Vesta, *Icarus* **127**, 1997, 130–157, http://dx.doi.org/10.1006/icar.1997.5680.

Garry W.B., et al., Geologic mapping of ejecta deposits in Oppia Quadrangle, Asteroid (4) Vesta, *Icarus* **244**, 2014, 104–119, http://dx.doi.org/10.1016/j.icarus.2014.08.046.

Jaumann R., et al., Vesta's shape and morphology, *Science* **336** (6082), 2012, 687–690, http://dx.doi.org/10.1126/science.1219122.

Kneissl T., et al., Geology of quadrangle Av-13 Tuccia, Vesta – Morphology and formation ages of mid-sized post-Rheasilvia craters, *Icarus* **244**, 2014, 133–157, http://dx.doi.org/10.1016/j.icarus.2014.02.012.

Le Corre L., et al., Olivine or impact melt: Nature of the "orange" material on Vesta from Dawn, *Icarus* **226**, 2013, 1568–1594, http://dx.doi.org/10.1016/j.icarus.2013.08.013.

Li, J.-Y., 2013. Body-fixed Coordinate Systems for Asteroid (4) Vesta. <http://sbn.psi.edu/archive/dawn/fc/DWNVFC2_1A/DOCUMENT/VESTA_COORDINATES/VESTA_COORDINATES_131018.PDF>.

Li J.-Y., et al., Photometric mapping of Asteroid (4) Vesta's southern hemisphere with Hubble Space Telescope, *Icarus* **208**, 2010, 238–251, http://dx.doi.org/10.1016/j.icarus.2010.02.008.

Longobardo A., et al., Photometric behavior of spectral parameters in Vesta dark and bright regions as inferred by the Dawn VIR spectrometer, *Icarus* **240**, 2014, 20–35, http://dx.doi.org/10.1016/j.icarus.2014.02.014.

Longobardo, A. et al., 2015. Mineralogical and spectral analysis of Vesta's Gegania and Lucaria quadrangles and comparative analysis of their key features. Icarus (this issue)-, http://dx.doi.org/10.1016/j.icarus.2015.04.031.

McCord T.B., et al., Dark material on Vesta from the infall of carbonaceous volatile-rich material, *Nature* **491** (7422), 2012, 83–86, http://dx.doi.org/10.1038/nature11561.

McFadden, L.A. et al., 2015. Vesta's Pinaria Region: Original basaltic achondrite material derived from mixing upper and lower crust. Icarus (this issue).

McSween H.Y., et al., Composition of the Rheasilvia basin, a window into Vesta's interior, *J. Geophys. Res.: Planets* **118** (2), 2013, 335–346, http://dx.doi.org/10.1002/jgre.20057.

Mittlefehldt, D.W. et al., 2012. Types and distribution of bright materials on 4 Vesta. Lunar Planet. Sci. 43. LPI Contribution No. 1659, id. 1680.

Palomba E., et al., Composition and mineralogy of dark material units on Vesta, *Icarus* **240**, 2014, 58–72, http://dx.doi.org/10.1016/j.icarus.2014.04.040.

Pieters C.M., et al., A sharper view of impact craters from Clementine data, *Science* **266** (5192), 1994, 1844–1848, http://dx.doi.org/10.1126/science.266.5192.1844.

Pieters C.M., et al., *Nature* **491** (7422), 2012, 79–82, http://dx.doi.org/10.1038/nature11534.

Reddy V., et al., Color and albedo heterogeneity of Vesta from Dawn, *Science* **336** (6082), 2012, 700–704, http://dx.doi.org/10.1126/science.1219088.

Reddy V., et al., Comparing Dawn, Hubble Space Telescope, and ground-based interpretations of (4) Vesta, *Icarus* **226**, 2013, 1103–1114, http://dx.doi.org/10.1016/j.icarus.2013.07.019.

Roatsch T., et al., High resolution Vesta High Altitude Mapping Orbit (HAMO) atlas derived from Dawn Framing Camera images, *Planet. Space Sci.* **73**, 2012, 283–286, http://dx.doi.org/10.1016/j.pss.2012.08.021.

Ruesch O., et al., Detections of the near-IR spectral signature of olivine on Vesta with VIR/Dawn data: Insights into Vesta olivine-bearing lithologies, *J. Geophys. Res.: Planets* **119** (9), 2014, 2078–2108, http://dx.doi.org/10.1002/2014JE004625.

Russell C.T., et al., Dawn at Vesta: Testing the protoplanetary paradigm, *Science* **336** (6082), 2012, 684–686, http://dx.doi.org/10.1126/science.1219381.

Schäfer M., et al., Imprint of the Rheasilvia impact on Vesta – Geologic mapping of quadrangles Gegania and Lucaria, *Icarus* **244**, 2014, 60–73, http://dx.doi.org/10.1016/j.icarus.2014.06.026.

Schröder S.E., et al., Resolved photometry of Vesta reveals physical properties of crater regolith, *Planet. Space Sci.* **85**, 2013, 198–213, http://dx.doi.org/10.1016/j.pss.2013.06.009.

Shkuratov Yu.G., et al., Opposition effect from Clementine data and mechanisms of backscatter, *Icarus* **141**, 1999, 132–155, http://dx.doi.org/10.1006/icar.1999.6154.

Sierks H., et al., The Dawn Framing Camera, *Space Sci. Rev.* **163** (1–4), 2011, 263–327, http://dx.doi.org/10.1007/s11214-011-9745-4.

Stephan K., et al., A compositional and geologic view of fresh ejecta of small impact craters on Asteroid 4 Vesta, *J. Geophys. Res.: Planets* **119** (4), 2014, 771–797, http://dx.doi.org/10.1002/2013JE004388.

Stephan, K. et al., 2015. The Sextilia region on Asteroid 4 Vesta – Stratigraphy and variegation. Icarus (this issue)-, http://dx.doi.org/10.1016/j.icarus.2015.05.016.

Tosi F., et al., Thermal measurements of dark and bright surface features on Vesta as derived from Dawn/VIR, *Icarus* **240**, 2014, 36–57, http://dx.doi.org/10.1016/j.icarus.2014.03.017.

Williams D.A., et al., The geology of the Marcia quadrangle of asteroid Vesta: Assessing the effects of large, young craters, *Icarus* **244**, 2014a, 74–88, http://dx.doi.org/10.1016/j.icarus.2014.01.033.

Williams D.A., et al., The chronostratigraphy of protoplanet Vesta, *Icarus* **244**, 2014b, 158–165, http://dx.doi.org/10.1016/j.icarus.2014.06.027.

Zambon F., et al., Spectral analysis of the bright materials on the Asteroid 4 Vesta, *Icarus* **240**, 2014, 73–85, http://dx.doi.org/10.1016/j.icarus.2014.04.037.

Zambon, F. et al., 2015. Spectral analysis of the quadrangles Av-13 and Av-14 on Vesta. Icarus (this issue)-, http://dx.doi.org/10.1016/j.icarus.2015.05.015.

Footnotes

[1]Let i, e, and p be the incidence, emission, and phase angles of a FC map pixel. Then the corrected reflectance is: corrected_reflectance = (I/F)_Akimov($i = 30°$, $e = 0°$, $p = 30°$) × (I/F)_observed(i, e, p)/(I/F)_Akimov(i, e, p) where "(I/F)_Akimov(i, e, p)" and "(I/F)_observed(i, e, p)" are the modeled and observed I/F, respectively. The model value is calculated for the particular geometry (i, e, p) of the observation. Ultimately, the corrected reflectance is normalized to the predicted I/F at the standard angle of $i = 30°$, $e = 0°$ ($p = 30°$).

Highlights

- The older northeastern part of Av-10 is dominated by howardite-like material.
- The younger southwestern part (including Oppia) has a markedly eucritic mineralogy.
- Oppia crater itself displays considerable spectral variability in its interior.
- OH-rich material mostly correlate with Oppia's ejecta.
- Substantial hydration is found in moderate-albedo, light mantle material west of Oppia.

Queries and Answers

Query: Your article is registered as belonging to the Special Issue/Collection entitled "Vesta Surface Composition". If this is NOT correct and your article is a regular item or belongs to a different Special Issue please contact dikea@elsevier.com immediately prior to returning your corrections.
Answer: This article belongs to a special issue on the mineralogical mapping of Vesta's quadrangles, initially indicated as a special issue on "Vesta surface composition". There is no error.

Query: Please confirm that given name(s) and surname(s) have been identified correctly.
Answer: Surnames have been checked and are all correct.

Query: References 'McCord et al. (1970) and De Sanctis et al. (2014)' are cited in the text but not provided in the reference list. Please provide them in the reference list or delete these citations from the text.
Answer: McCord, T.B., Adams, J.B., Johnson, T.V., 1970. Asteroid Vesta: Spectral reflectivity and compositional implications. Science 168, Issue 3938, 1445-1447. Doi: 10.1126/science.168.3938.1445. De Sanctis, M.C., Ammannito, E., Buczkowski, D., Raymond, C.A., Jaumann, R., Mittlefehldt, D.W., Capaccioni, F., Capria, M.T., Frigeri, A., Magni, G., Tosi, F., Zambon, F., Russell, C.T., 2014. Geophys. Res. Lett. 41, Issue 9, 3038-3044. Doi: 10.1002/2014GL059646.

Query: One or more sponsor names may have been edited to a standard format that enables better searching and identification of your article. Please check and correct if necessary.
Answer: Italian Space Agency is correct. There is no oversight here.

Query: Please provide article title for references 'Ammannito et al. (2013) and Pieters et al. (2012)'.
Answer: Title for Ammannito et al. (2013) is: "Olivine in an unexpected location on Vesta's surface". Title for Pieters et al. (2012) is: "Distinctive space weathering on Vesta from regolith mixing processes".

Query: Please note that 'blue and red colors' has been changed to 'bold and bolditalic', and correct if necessary.
Answer: I understand that the change in style, from blue and red colors to bold and bolditalic, is due to an editorial constraint. If this cannot be handled otherwise, I am fine with this change.

Query: The country names of the Grant Sponsors are provided below. Please check and correct if necessary. 'Italian Space Agency' - 'Italy'.
Answer: No, please let this Grant Sponsor be indicated as: "Italian Space Agency (ASI)", just as it is now.